RMIT UNIVERSITY

An Investigation of New Ionospheric Models Using Multi-source Measurements and Neural Networks

A thesis submitted in fulfilment of the requirements for the degree of *Doctor of Philosophy*

Andong Hu

Bachelor of Engineering (BEng) from Nanjing University of Information Science and Technology, China

School of Science

College of Science, Engineering and Health

RMIT University

October 2019

Doctoral Citation

Dr Hu developed an innovative earth-ionosphere model using machine learning methods based on multi-source measurements. The research produced several sub-models which targets different ionospheric parameters using different machine learning techniques. These findings improve the accuracy of the prediction and enhance our understanding for the physical mechanisms of the ionosphere.

Declaration

I certify that except where due acknowledgement has been made, the work is that of the author alone; the work has not been submitted previously, in whole or in part, to qualify for any other academic award; the content of the thesis is the result of work which has been carried out since the official commencement date of the approved research program; any editorial work, paid or unpaid, carried out by a third party is acknowledged; and, ethics procedures and guidelines have been followed.

Andong Hu
7 October 2019

Acknowledgements

Firstly, I would like to express my sincere gratitude to my supervisors, Prof Kefei Zhang, Dr Brett Carter, Dr Julie Currie, Dr Robert Norman and Dr Suqin Wu, for their full support, encouragement, and guidance throughout my PhD study. They spent countless hours proofreading my research papers and providing valuable suggestions, which always result in significant improvements in the quality of the thesis and refinement of my research. What I have learnt from them is not only vital for the accomplishments achieved during the period of my PhD study but also very beneficial to my future career.

I am also grateful to the help and friendship from those colleagues at the SPACE Research Centre or the project team members, including A/prof. Suelynn Choy, Dr Pawel Hordyniec, Dr Yubin Yuan, Dr Fu Chen, Dr Zishen Li, Dr Li Li, Dr Jianqiang Wang, and many others at RMIT. My thanks also go to my lab-mates and fellow students for all their supports and fun we had together in the last four years. They are Dr Yuntian Brian Bai, Dr Xiaoming Wang, Dr Changyong He, Dr Han Cai, Dr Yang Yang, Dr Yaguang Tao, Dr Yang Zhao, Mr Micheal Andoh Afful, Dr Timothy Kodikara, Ms Yeasmin Alea, Ms Samantha Le May, Mr Viet Duong and Mr Nenad Radosevic. I would like to acknowledge my master's supervisor, Prof Jian Wang, who continues giving me his valuable advice and help.

My PhD work has been financially supported by the Chinese Scholarship Council, Cooperative Research Centre for Space Environment (SERC Limited) through the Australian Government's Cooperative Research Centre Programme and Australian Bureau of Meteorology Linkage project through Australian Research Council. Dr. Steve Gower and Michelle Fulton are thanked for their help during my PhD study.

Last but not the least, I must express my very profound gratitude to my parents and my lovely girlfriend for their unreserved love and continuous encouragement throughout all my years of study, the process of research and thesis writing. This accomplishment would not have been possible without their support. Thank you all.

Abbreviations

ANN Artificial Neural Network

AFRL Air Force Research Laboratory

Bi-LSTM Bidirectional Long Short-Term Memory

BoM Australian Bureau of Meteorology

BVBLS Base-Vector-Based Least Squares

COSMIC Constellation Observing System for Meteorology, Ionosphere, and Climate

CAS Chinese Academy of Sciences

CHAMP Challenging Minisatellite Payload

CDAAC COSMIC Data Analysis and Archive Centre

DNN Deep Neural Network

DoY Day of Year

EBP Equatorial Plasma Bubble

EDP Electron Density Profile

EIA Equatorial Ionisation Anomaly

GRACE Gravity Recovery and Climate Experiment

GRACE-FO Gravity Recovery and Climate Experiment Follow-On

GNSS Global Navigation Satellite Systems

GPS Global Positioning System

GIM Global Ionosphere Map

GIPP Group of Ionosphere and Precise Positioning based on BDS/GNSS

GFZ Germany's National Research Centre for Geosciences

HF high frequency

ISR Incoherent Scatter Radar

IRI International Reference Ionosphere

IGS International GNSS Service

IAG International Association of Geodesy

JPL Jet Propulsion Laboratory

LSTM Long Short-Term Memory

LS Least Squares

LEO Low Earth Orbit

MSNA Mid-latitude Summer Nighttime Anomaly

NRL Naval Research Laboratory

NSPO Taiwaness National Space Organization

N_e Electron Density

NN Neural Network

RO Radio Occultation

RNN Recurrent Neural Network

T_e Electron Temperature

TS Topside Sounder

TECU Total Electron Content Unit

TIEGCM Thermosphere-Ionosphere-Electrodynamics General Circulation Model

UCAR University Corporation for Atmospheric Research

VSH Vertical Scale Height

VCE Variance Component Estimation

VTEC Vertical Total Electron Content

WTLS Weight Total Least Squares

Abstract

Ionosphere is one of the atmospheric layers that has a major impact on human beings since it significantly affects the radio propagation on Earth, and between satellites and Earth (e.g., Global Navigation Satellite Systems (GNSS) signal transmission). The variation of the electrons in the ionosphere is strongly influenced by the space weather due to solar and cosmic radiation. Hence, the short/long-term trend of the free electrons in the ionosphere has been regarded as very important information for both space weather and GNSS positioning.

On the other hand, precisely quantifying the distribution and variation of free electrons at a high spatio-temporal resolution is often a challenge if the number of the electrons (electron density) is detected only from the traditional ionospheric sensors (e.g., ionosonde and topside sounder and Incoherent Scatter Radar (ISR)) due to their low spatio-temporal coverage. This disadvantage is also inherited from the empirical ionospheric model developed based on these data sources. Nowadays, the availability of advanced observation techniques, such as GNSS Radio Occultation (RO) and satellite altimetry, for the measurement of Electron Density (N_e) and related parameters (e.g., $hmF2$, $NmF2$, Vertical Scale Height (VSH), Electron Density Profile (EDP) and Vertical Total Electron Content (VTEC)) in the ionosphere has heralded a new era for space weather research in the upper atmosphere. The new sources of data for ionospheric modelling can improve not only the accuracy but also the reliability of the model (such as[96] for $hmF2$ and [28] for VTEC).

In this study, Helmert Variance Component Estimation (VCE) aided Weight Total Least Squares (WTLS) is selected for modelling global VTEC using International GNSS Service stations, satellite altimetry and GNSS-RO measurements. The results show that the new VTEC model outperforms the traditional global ionospheric VTEC Model by at least 1.5 Total Electron Content Unit (TECU) over the ocean. This improvement is expected to be significant in the refinement of global ionospheric VTEC Model development.

As is well known, the most traditional models developed are prone to the effects of inherent assumptions (e.g. for the construction of the base functions in the models) which may lead to large biases in the prediction. In this study, an innovative machine learning technique (i.e. Neural Network (NN)) is investigated as the modelling method to address this issue. Different from the traditional modelling method, neither the observation equations (or

the so called 'design matrix'), nor apriori knowledge of the relationship (both of them can be considered as the source of the aforementioned assumptions) is required in the modelling process of a NN. This network system can automatically construct an optimal regression function based on a large amount of sample data and the designed network [43].

In this study, Deep Neural Network (DNN), which is an advanced Artificial Neural Network (ANN) (with more than one hidden layer), is investigated for their usability of VSH and topside EDP modelling, as well as the relationship between N_e and electron temperature. The results reveal that the new VSH model agrees better than the traditional model with regards to either out-of-sample measurements or the external reference (i.e. ISR data). In addition, the new model can represent the characteristic of VSH in the equatorial region better than that of traditional approaches during geomagnetic storms. The relationship between N_e and Electron Temperature (T_e) investigated from ISR data can be used to improve the performance of the current T_e model. The local time-altitude variation of the model outputs agrees well with that from a physical model (i.e., Thermosphere-Ionosphere-Electrodynamics General Circulation Model (TIEGCM)). The new topside EDP model takes $hmF2$ and $NmF2$ into consideration as part of the variable set. Comparing with the reference data (i.e., out-of-sample COSMIC data, GRACE and ISR data), the new model agrees much better than the International Reference Ionosphere (IRI)-2016 model. In addition, an advanced NN technique, Bidirectional Long Short-Term Memory (Bi-LSTM), is utilised to forecast $hmF2$ by using the $hmF2$ measured by Australian ionosondes in the five hours prior. The forecast results are better than the results from real-time models in the next five hours. The new model performs also better than the current $hmF2$ model (i.e., AMTB [2] and shubin [96] models, which is used inside IRI-2016 model) by at least 10km in most ionosonde stations.

Overall, the neural network technique has a great potential in being utilised in the ionospheric modelling. In addition to the accuracy improvement, the physical mechanism can be observed from the model outputs as well. In future work, the neural network is expected to be further applied in some other space weather studies (e.g., Dst, solar flare, etc).

LIST OF PUBLICATION

Appended papers

Paper A

Hu, A.; Wu, S.; He, C.; & Zhang, K. Four-dimensional Topside Electron Density Modelling using L2-ANN from GNSS-Ionospheric Radio Occultation Data, Submitted to Space Weather on May 3, 2019

Paper B

Hu, A., Carter, B., Currie, J., Norman, R., & Zhang, K. (2019). Modeling of Topside Ionospheric Vertical Scale Height Based on Ionospheric Radio Occultation Measurements. Journal of Geophysical Research:Space Physics, 124(6), 4926-4942. 10.1029/2018JA026280

Paper C

Hu, A., Li, Z., Carter, B., Wu, S., Wang, X., Norman, R., & Zhang, K. (2019). Helmert-VCE-aided fast-WTLS approach for global ionospheric VTEC modelling using data from GNSS, satellite altimetry and radio occultation. Journal of Geodesy, 93(6), 877-888. DOI: 10.1007/s00190-018-1210-7

Paper D

Hu, A., & Zhang, K. (2018). Using Bidirectional Long Short-Term Memory Method for the Height of F2 Peak Forecasting from Ionosonde Measurements in the Australian Region. Remote Sensing, 10(10), 1658. DOI: 10.3390/rs10101658

Paper E

Hu, A., Carter, B., Currie J., Norman, R., & Zhang, K. (2020). A Deep Neural Network Model of Global Topside Electron Temperature Using Incoherent Scatter Radars and Its Application to GNSS Radio Occultation. Journal of Geophysical Research: Space Physics, 125, e2019JA027263. DOI: 10.1029/2019JA027263

Other published papers

Hu, A., Wu, S., Wang, X., Wang, Y., Norman, R., He, C., ... & Zhang, K. (2018). Improvement of reflection detection success rate of GNSS RO measurements using artificial neural network. IEEE Transactions on Geoscience and Remote Sensing, 56(2), 760-769. DOI: 10.1109/TGRS.2017.2754512

Li, W., Yue, J., Yang, Y., He, C., **Hu, A.**, & Zhang, K. (2018). Ionospheric and Thermospheric Responses to the Recent Strong Solar Flares on 6 September 2017. Journal of Geophysical Research: Space Physics, 123(10), 8865-8883. DOI: 10.1029/2018JA025700

He, C., Wu, S., Wang, X., **Hu, A.**, Wang, Q., & Zhang, K. (2017). A new voxel-based model for the determination of atmospheric weighted mean temperature in GPS atmospheric sounding. Atmospheric Measurement Techniques, 10(6). DOI: 10.5194/amt-10-2045-2017

Bai, Y. B., Gu, T., & **Hu, A.** (2016, October). Integrating Wi-Fi and magnetic field for fingerprinting based indoor positioning system. In 2016 International Conference on Indoor Positioning and Indoor Navigation (IPIN) (pp. 1-6). IEEE. DOI: 10.1109/IPIN.2016.7743699

Table of contents

LIST OF PUBLICATION **xiii**

List of figures **xvii**

List of tables **xix**

1 Introduction **1**
1.1 Background and Motivations 1
1.2 Research Aims and Objectives 4
1.3 Thesis Structure 5

2 Data and Methods **7**
2.1 Data 7
2.1.1 International GNSS Service (IGS) 7
2.1.2 GNSS-Radio Occultation (GNSS-RO) 8
2.1.3 Satellite Altimetry 9
2.1.4 Ionosonde (in Australian region) 9
2.1.5 Incoherent Scatter Radar (ISR) 10
2.2 Methods 11
2.2.1 Deep Neural Network (DNN) 11
2.2.2 Recurrent Neural Network (RNN) 14
2.2.3 Helmert Variance Component Estimation Aided fast-Weighted Total Least Squares (Helmert-VCE-Aided fast-WTLS) 19
2.3 Summary 19

3 Topside Electron Density Modelling using DNN from GNSS RO Data **21**
3.1 Introduction 21
3.2 Paper A: Four-dimensional Topside Electron Density Modelling using L2-ANN from GNSS-Ionospheric Radio Occultation Data 23

3.3 Summary 23

4 Investigation of Topside VSH Based on GNSS-RO Measurements 25
4.1 Introduction 25
4.2 Paper B: Modeling of Topside Ionospheric Vertical Scale Height Based on Ionospheric Radio Occultation Measurements 27
4.3 Summary 27

5 A New GIM Developed by Helmert-VCE-Aided fast-WTLS Method from Multi-Source of Data 29
5.1 Introduction 29
5.2 Paper C: Helmert-VCE-Aided fast-WTLS Approach for Global Ionospheric VTEC Modelling Using Data from GNSS, Satellite Altimetry and Radio Occultation 31
5.3 Summary 31

6 Using Bi-LSTM Method for hmF2 Forecasting from Ionosonde Measurements in Australian Region 33
6.1 Introduction 33
6.2 Paper D: Using Bidirectional Long Short-Term Memory Method for the Height of F2 Peak Forecasting from Ionosonde Measurements in the Australian Region 35
6.3 Summary 35

7 Global Topside Electron Temperature Modelling from ISR Measurements 37
7.1 Introduction 37
7.2 Paper E: A Deep Neural Network Model of Global Topside Electron Temperature Modeling Using Incoherent Scatter Radars and Its Application to GNSS Radio Occultation 39
7.3 Summary 39

8 Summary, Conclusion and Recommendation 41
8.1 Summary and Conclusion 41
8.2 Future work 42

References 45

List of figures

2.1 Distribution of the 12 ionosonde stations in the Australian region. 10

2.2 Three layers of DNN: input (blue); hidden (yellow) and output (green) layers. 'a's are the values of each cell (the round boxes in figure). The superscript of 'a' represents the index of the layer and the subscript of 'a' represents the index of the cell in that specific layer. '$a_0^{(l)}$'s denote the bias units in each layer ('l' is the index of the layer). $\Theta^{(l)}$ is the cluster of all 'θ's on the linkage between the $(l-1)$th layer and the lth layer, and $\theta_{nm}^{(l)}$ means the coefficient between the nth cell in the $(l-1)$th layer and the mth cell in the lth layer. x and $h_\theta(x)$ are the input and output of the system respectively. In addition, $g^{(l)}$ is the activation function for the lth layer and $h_\theta(x)$ is the symbol for the whole DNN fitting model. 13

2.3 Flowchart showing the process to obtain a regression model using DNN. The greyed parallelograms indicate the section of the dataset used at each stage in the process, white rectangles indicate the processes, white diamonds indicate the questions that control the following steps and the white cylinder is the final DNN derived model. 15

2.4 Structure of RNN. X_t is the independent variable set at the tth epoch, and Y is the independent variable. h_t is the temporary results from the tth RNN unit, h_0 is manually initialised. The connection between h and Y are normal softmax/regression. Each RNN unit can be considered as an ANN model (Fig. 2.2). 'W's and 'b's are the coefficients and biases that need to be estimated during the training. In addition, H is the *Tanh* function. 16

2.5 Structure of the LSTM. Similar to RNN (Fig 2.4) but with memory cell c added. i, f, o are the input gate, forget gate and output gate respectively. σ is the *Sigmoid* function. 17

2.6 Structure of the bi-LSTM method, similar to the LSTM method (Fig 2.5), the training is carried out in both directions (i.e. both sequential forward and sequential backward). 18

List of tables

2.1 Australian ionosonde stations and their geographic coordinates 11
2.2 Number of sample data from seven ISR stations 11

Chapter 1

Introduction

1.1 Background and Motivations

"Space weather" is a branch of space physics and aeronomy, or heliophysics, which is concerned with the time-varying conditions within the solar system. It emphasises the space surrounding the Earth, including the solar wind, the magnetosphere, the ionosphere, and the thermosphere. Space weather can influence the reliability of space-borne and ground-based observation systems and even endanger human lives. Extreme space weather conditions in the space environment can cause significant disruption of satellite operations, communication, navigation, and power distribution grids, leading to colossal economic losses [78].

Space weather conditions can be observed/revealed by the behaviour of the ionised plasma in the upper atmosphere which is usually defined as the region between 80km and 2000km. At this altitude, the density of neutral particles is low enough to free electrons. It can be done through ionisation which is a process of making positively or negatively charged atoms or molecules by adding or stripping away one or more electrons. Ionisation is much more common in the upper atmosphere because it is mostly caused by either high-energy photons (mostly UV and X-rays) or energetic particles (from either solar wind or cosmic radiation) that penetrate into the atmosphere and collide with the surrounding gas. The peak number of free ions and electrons (so-called '$NmF2$') usually occurs at an altitude around 300km (so-called '$hmF2$'). The region surrounding this peak (in electron density) is called the ionosphere (i.e. 80km-2000km above the earth). Therefore, the space weather events can be forecast by analysing the variation of these ionospheric parameters (such as $hmF2$ and $NmF2$).

In addition to space weather research, our daily life activities can also be affected by the ionospheric irregularities such as scintillations (in both low and high latitudes), plasma bubbles (mostly in lower latitudes, so-called 'Equatorial Plasma Bubble (EBP)') and large

scale travelling ionospheric disturbances (mainly observed at high latitudes) [25]. For example, the ionospheric anomalies affect GNSS signals as the signals transmitted through the ionosphere which can lead to huge positioning errors, and in the worst scenario, it can completely lose track to the GNSS satellites. Although the first-order ionospheric delay can be removed by using dual-frequency receivers, it is not enough to eliminate the entire influence of the ionosphere, especially in an extreme space weather event which may cause a non-negligible high order ionospheric refraction effect [52]. Furthermore, strong geomagnetic storms are also known to cause a complete blackout of radio communications because at that time the ionosphere will be a complete mess. Therefore, modelling and forecasting the variation of the electrons in the ionosphere can be beneficial to both space weather analyses and solving real world problems (e.g., N_e and VTEC can help mitigate the GNSS positioning errors).

In addition to the aforementioned $hmF2$ and $NmF2$, several other essential ionospheric parameters are also investigated in this study, including N_e, VTEC, VSH and T_e. N_e is the number of the electrons presented at a specific location and T_e is the energy carried by these electrons. VTEC is the total number of electrons in a vertical cube from the earth surface to the upper boundary of the ionosphere (cross-section area is $1m^2$). VSH is generally defined as the value of $dh/d(ln(N_e))$ by relating to the gradient of the topside N_e profile [61]. All of these data (except T_e) can be obtained from an N_e vertical profile. Based on the relationship between N_e and T_e, T_e can be retrieved from the profile as well.

A number of instruments have been used to measure the N_e profiles. They can be broadly divided into two categories: ground-based (e.g., ISRs [62] and ionosondes [83, 62]) and satellite-based (e.g., topside sounder satellites [20, 9] and GNSS-RO satellites [92, 116, 97, 21–23]). Currently, the most frequently used N_e data are measured by ionosonde and have been collected since the early 20th century. There are hundreds of ionosonde stations operating at the same time all over the globe, and each station can provide N_e measurements in a 15-30 minutes interval. The flip side of the ionosonde measurements is that it cannot measure N_e profiles in the topside ionosphere (above $hmF2$) which plays a very important role in the ionospheric study. In contrast, Topside Sounder (TS) satellites can measure the topside ionosphere, but not the bottomside. ISRs and GNSS-RO satellites can measure N_e in both the bottomside and topside of the ionosphere [77, 21, 22]. Although ISR by far is the most powerful ground-based remote-probing tool for the study of the ionospheric process [62], the horizontal coverage of ISR is too limited (the window of sky view over an ISR is very small) to be adopted for global modelling.

The GNSS-RO is a relatively new and interesting atmospheric sounding technique [44, 85, 118, 86, 111]. It is based on the fact that the L-band radio signals are refracted in

the atmosphere during the transmission from a GNSS satellite to a Low Earth Orbit (LEO) satellite. The idea of GNSS-RO is to retrieve atmospheric parameters (e.g.,refractivity and water vapour) in the neutral atmosphere [85] from the bending angles of the radio signals and ionospheric parameter from calibrated phases (related to the L1-L2 phases) [44]. More importantly, GNSS-RO can provide long-term (low-cost) worldwide atmospheric profiles with a high vertical resolution in comparison with other traditional atmospheric sounding techniques. The quality of GNSS-RO products has been investigated and confirmed by many researches [64, 100, 117, 36, 37]. Hence, GNSS-RO data are selected as the main source of data in this study (sometimes assisted by other sources of data).

Ionospheric information can also be obtained from the ionospheric model [9] based on either empirical function (e.g., Vary-Chap function [81] in the IRI) or physical mechanism (e.g., the equations inside TIEGCM [67]). However, ionospheric information from both methods is prone to the effect of inherent assumptions in the models which leads to potential bias problem in the prediction. Hence, the results from the both types of the models are only used for comparison in this study.

The bias of physical ionospheric model (like the aforementioned TIEGCM) is mostly caused by the fact that the complicated physical mechanism of the ionosphere is impossible to be described thoroughly by current equations. The exact relationship between independent variable and ionospheric information remains unknown. To address this issue, NN method is utilised for the ionospheric studies. The NN was initially inspired by biological neural systems for regression or classification for an unknown function based on a large amount of input/training data. Nowadays, the NN has been widely used in many fields, e.g. data mining [18], automatic driving [33], and even atmospheric modelling [53, 55, 88]. It is well-known that a set of observation equations (or so-called “design matrices”) need to be designed first in the traditional Least Squares (LS) estimation method for regression modelling [74]. The design matrices are generally based on the assumed relationships between the dependent and independent variables (the relationship is also called "base function"). However, as is mentioned above, some of the exact relationships are unknown. Fortunately, neither the observation equations nor the apriori knowledge of the relationship is required for the NN modelling. This NN system can automatically construct the optimal regression function based on the sample data and the designed network [43]. Thus, in this study, different NN methods are utilised to different applications to take new physical features into consideration for ionospheric modelling. In addition, for those models whose base function is well known and widely used (i.e., spherical harmonics for GIM), advanced modelling methods, i.e. Helmert-VCE-aided weight total least squares (Helmert-VCE-aided WTLS), is applied to not

only consider the bias among various sources of data but also adjust the error in the design matrix as well.

1.2 Research Aims and Objectives

The major aims of this research are to develop new global/regional ionospheric models (in both spatial and temporal domains) to nowcast/forecast various essential ionospheric parameters by utilising advanced neural networks and some other cutting-edge modelling methods from multi-source data. In addition to the space weather analysis, these models can be also applied to mitigate the interference to GNSS usages at the second order (dual-frequency receivers) in real-time/near-real-time. The specific objectives of the research are:

- to develop new VSH and topside N_e models from COSMIC using DNN, an advanced ANN) algorithm and the models' performance are then assessed with regards to both out-of-sample data and an external reference (i.e. ISR in this study) in comparison with the traditional empirical models.
- to investigate the relationship between N_e and T_e by using global ISR measurements (from three ISR stations on behalf of low, mid and high latitude regions respectively) and generate corresponding topside T_e from Constellation Observing System for Meteorology, Ionosphere, and Climate (COSMIC) N_e profile based on the new N_e-T_e model. A comparison has been made between the model results and TIEGCM outputs (it should be noted that it is just a comparison since no ground true for T_e in global coverage can be considered as the reference).
- to develop a new global ionospheric VTEC model based on IGS, Jason-3 and COSMIC data using Helmert-VCE-aided WTLS method. The model results are compared with three traditional VTEC global models with reference to the out-of-sample observations.
- to forecast Australian hmF2 in the next hour by using the hmF2 in the past five hours based on ionosonde measurements and the Bi-LSTM method.
- to investigate if the physical characteristics of the ionosphere can be captured by the proposed models' output (e.g., Mid-latitude Summer Nighttime Anomaly (MSNA) and Equatorial Ionisation Anomaly (EIA)).

1.3 Thesis Structure

Chapter 2 introduces the source of data and the methods utilised in this research in detail.

Chapter 3 (paper A) develops a topside N_e model from GNSS-RO data. The model takes hmF2 and NmF2 into consideration as part of the variable set. The performance of the new model is then evaluated by comparing with IRI-2016 model using the out-of-sample COSMIC data as well as GRACE and ISR data as references. Whether the ionospheric characteristics (i.e., EIA and MSNA) can be captured by the model outputs is also validated in this chapter.

Chapter 4 (paper B) proposes a new VSH model from GNSS-RO data using the DNN method. The new model agrees well with both out-of-sample GNSS-RO data and the external reference (i.e. ISR data) better than the traditional model. In addition, the new model agrees with the characteristic of VSH in the equatorial region better than traditional approach during geomagnetic storm times as well. It suggests that the new VSH model may be able to be used in space weather analysis and prediction even during extreme conditions.

Chapter 5 (paper C) introduces a new VTEC Global Ionosphere Map (GIM) developed by using Helmert-VCE-aided WTLS method from multiple source data. It is the first time to utilise WTLS in the GIM (or even ionospheric) modelling. In this chapter, the proposed VTEC model was tested using the data in the period of Day of Year (DoY) 217-224, 2016 and validated using GIMs produced by the other research centres, such as Group of Ionosphere and Precise Positioning based on BDS/GNSS (GIPP) at the Academy of Opto-Electronics, Chinese Academy of Sciences (CAS).

Chapter 6 (paper D) forecasts hmF2 in the Australian region up to five hours from ionosonde data using the Bi-LSTM method. Various assessments have been conducted by comparing the new model with the traditional hmF2 model (i.e., AMTB, Shubin, also ANN and Long Short-Term Memory (LSTM) models). In addition to the space weather prediction, this model possibly can be utilised for the validation of the auto-scaled ionosonde data.

Chapter 7 (paper E) investigates a better relationship (closer to the reality) between N_e and T_e using both DNN method and the ISR measurements which haven't been improved since 1980s. The results generated by the model and GNSS-RO (as the input) are then compared with TIEGCM for investigating whether the model can capture the characteristics of T_e in both spatial and temporal domains.

Chapter 8 gives a summary and conclusion of this research and prospect for future work.

Chapter 2

Data and Methods

This section introduces all the data and methods (algorithms) adopted in the chapter to be followed for a better understanding of the ionospheric models developed in this research. The data subsection includes the data used as either samples or references. The methods section contains the algorithm used for developing either the new model or the model for comparison.

2.1 Data

2.1.1 International GNSS Service (IGS)

IGS, established by the International Association of Geodesy (IAG) in June 1994, was initially known as International Global Positioning System (GPS) Service. The name of IGS from GPS to GNSS was changed in March 2005, when it was freely available for high precision GNSS satellite users [5]. Until May 2017, a total of more than 500 stations exist in the IGS network all over the world [35] as is shown in Fig. 3(a) in [54]. The highest quality of GNSS data in support of research, earth observation, and the terrestrial reference frame has been provided by IGS. The society has been significantly benefited, particularly in the areas of navigation, timing, and some other scale applications. A closely related product of the IGS is the GIM contains the two-hourly maps of global VTEC estimated from the permanent tracking sites which becomes a trustworthy source for ionospheric information since 1998.

2.1.2 GNSS-Radio Occultation (GNSS-RO)

The GNSS-RO is a relatively new and cutting-edge atmospheric sounding technique [44, 85]. It is based on the fact that the L-band GNSS signals are refracted in the atmosphere during the transmission from a GNSS satellite to an LEO satellite. The idea of GNSS-RO is to retrieve atmospheric parameters in both the neutral atmosphere [85, 113, 65] and ionosphere [44, 68] from the excess phases (related to the L1-L2 phases). More importantly, GNSS-RO can provide long-term (low-cost) worldwide atmospheric profiles with a high vertical resolution, in comparison with other traditional atmospheric sounding techniques.

Among all the GNSS-RO missions launched to date, two of them (i.e. COSMIC and Gravity Recovery and Climate Experiment (GRACE)) listed below can provide qualified ionospheric measurements through the COSMIC Data Analysis and Archive Centre (CDAAC). It should be noted that Challenging Minisatellite Payload (CHAMP) is not discussed in this study since it is no longer operational since 2010. COSMIC and GRACE are briefly introduced below:

1. COSMIC is a program designed to provide advances in meteorology, ionospheric research, climatology, and space weather by using GPS satellites in conjunction with LEO satellites. The term "COSMIC" may refer to either the organisation itself or the constellation of satellites (also known as FORMOSAT-3 in Taiwan). The constellation is a joint U.S.-Taiwan mission with major participants including the University Corporation for University Corporation for Atmospheric Research (UCAR), the National Science Foundation, the Naval Research Laboratory (NRL), the Air Force Research Laboratory (AFRL) on the U.S. side and the Taiwaness National Space Organization (NSPO) on the Taiwanese side. COSMIC is one of the most powerful GNSS-RO missions and its constellation consists of six LEO micro-satellites launched in April, 2006 [91, 64]. About 2000 N_e profiles per day were obtained in the initial operational stage (2006-2010), but it decreased considerably after 2010 (to around 1000 events per day).
2. The GRACE was a joint mission of NASA and the German Aerospace Centre. Twin satellites took detailed measurements of Earth's gravity field anomalies from its launch in March 2002 to the end of its scientific mission in October 2017. The Gravity Recovery and Climate Experiment Follow-On (GRACE-FO) is a continuation of the mission with near-identical hardware, launched in May 2018. GRACE was a collaborative endeavour involving the Center for Space Research at the University of Texas at Austin, NASA's Jet Propulsion Laboratory (JPL), the German Aerospace Centre and Germany's National Research Centre for Geosciences (GFZ), Potsdam. The measurements from the GRACE satellites are an important tool for studying the

Earth's ocean, geology, and climate. GRACE-A continuously provided ionospheric radio occultation data since the DoY 059, 2007 (February 28, 2007) until October 31, 2017 [6].

2.1.3 Satellite Altimetry

Altimetry is a technique for measuring height. Satellite altimetry measures the time taken by a radar pulse to travel from the satellite antenna to the surface and back to the satellite receiver. Combined with precise satellite location data, altimetry measurements yield sea-surface heights and can obtain fundamental information for tides. Jason-3 mission is one of the latest satellite altimetry missions and can provide worldwide VTEC data. With a 66° orbital inclination and a 1,336 km altitude, the trajectories of the satellite cover the latitudinal range from 66°N to 66°S. It should be noted that the polar regions are not measured. There are two bands used in Jason-3 measurements: Ku-band (main band, frequency is 13.575 GHz) and a C-band (auxiliary band, frequency is 5.3 GHz). The VTEC is mostly derived from Ku-band measurements.

VTEC can be calculated by following equation:

$$VTEC = -\frac{dR \times f^2}{40.28} \tag{2.1}$$

where f is the frequency of the Ku-band and dR is the Ku-band ionospheric range correction provided by the output of Jason-3 directly.

The onboard radar altimeters can directly access the differential ionospheric delay of the transmitted signals which can be used as an ionospheric correction. The error or uncertainty is usually no larger than 2–3 TECU. Each Jason-3 measurement is considered having equal quality in this study, thereby their initial weights are set to the same value.

2.1.4 Ionosonde (in Australian region)

The ionosonde instrument was prototyped in 1925 and further enhanced in the late 1920s. An ionosonde typically consists of four parts: a high frequency (HF) radio transmitter; a HF receiver; an antenna with a suitable radiation pattern; and a central control and data processing system. There are more than 100 ionosonde stations deployed around the world that routinely measure the structure and variability of bottomside ionosphere using the reflection of radio waves (echo sounding) [79]. hmF2 is the peak altitude of the detection range. There are 12 ionosonde stations in Australian region (see Figure 2.1). The geographic location and operational period of these stations are detailed in Table 2.1 which suggests that

they can provide enough samples for the proposed modelling work. In order to obtain stable quiet-time hmF2, monthly median hmF2 for each local hour (derived by using Eqn. (1)-(5) in [56] from various ionosonde measurements. The measurements are provided (manually scaled) by the Australian Australian Bureau of Meteorology (BoM) and it can be downloaded from ftp://ftp-out.sws.bom.gov.au/wdc/iondata/medians/) selected as the samples.

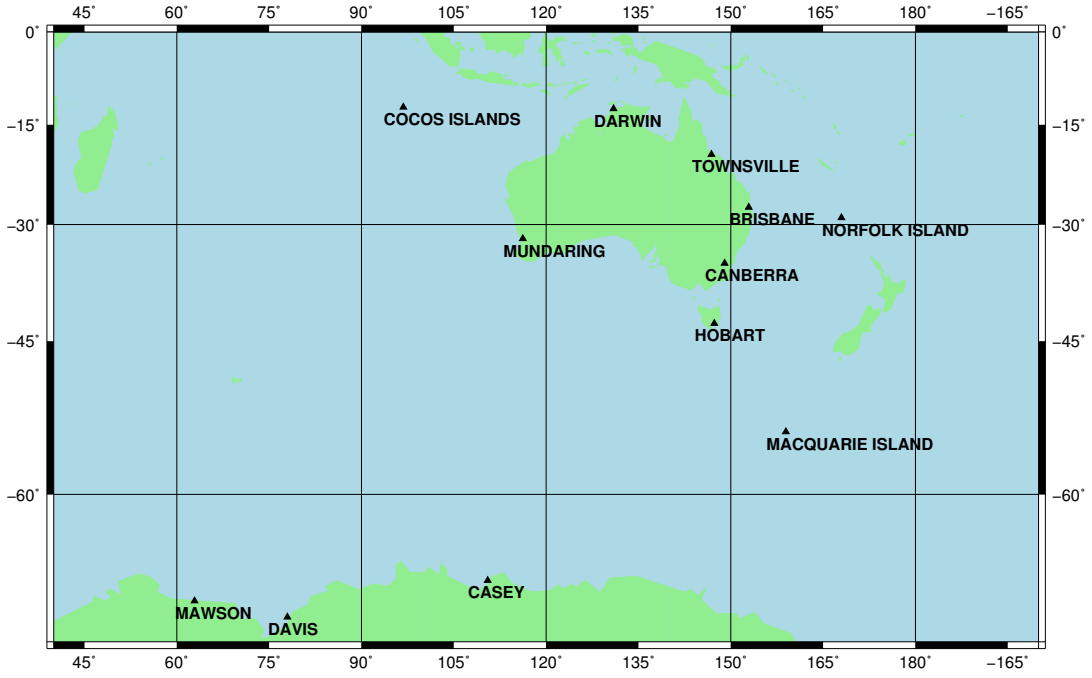

Fig. 2.1 Distribution of the 12 ionosonde stations in the Australian region.

2.1.5 Incoherent Scatter Radar (ISR)

ISR is a powerful instrument capable of simultaneously measuring the range-resolved ionospheric and atmospheric parameters [41, 32, 122, 58, 119, 63], including electron densities as well as the ion/electron temperature profiles, from the lower ionosphere up to the topside ionosphere. There are around 20 ISR stations arranged all over the globe. Only a few of them were used to measure N_e and T_e in upper atmosphere simultaneously (e.g., Arecibo, Millstone Hill, Poker Flat, etc). The location of these six ISR stations as examples is shown in Tab. 2.2, along with the number of sample data measured by each station. Arecibo, Millstone Hill and Poker Flat are selected representing the low, mid and high latitude regions respectively.

Table 2.1 Australian ionosonde stations and their geographic coordinates

Acronym (Station Name)	Latitude	Longitude	Open	Closed
CI (Cocos Islands)	-12.20	96.80	Nov 1961 Aug 2008	Sep 1974
DW (Darwin)	-12.45	130.95	Dec 1982	
TS (Townsville)	-19.63	146.85	Jun 1946	
BB (Brisbane)	-27.53	152.92	Jun 1943 Jun 1997	Dec 1986
NI (Norfolk Island)	-29.03	167.97	Feb 1964	
MD (Mundaring)	-31.98	116.22	Apr 1959	Dec 2007
CB (Canberra)	-35.32	149.00	Mar 1937	
HB (Hobart)	-42.92	147.32	Dec 1945	
MI (Macquarie Islands)	-54.50	158.95	Jun 1950 Nov 1983	Nov 1958 Jun 2015
CA (Casey)	-66.30	110.50	Jul 1957 Apr 1989 Nov 2000	Jan 1975 Mar 1992
MS (Mawson)	-67.60	62.88	Feb 1958	
DA (Davis)	-68.58	77.96	Feb 1985	

Table 2.2 Number of sample data from seven ISR stations

Region	Station	Geog-lat	Number of sample events
Low-lat	ARECIBO	18.3	193,012
	JICAMARCA	11.9	1,727
Mid-lat	MILLSTONE	42.6	106,928
	KHARKOV	50.0	3,645
	POKER FLAT	74.8	28,981
High-lat	SONDRE STROMFJORD	73.2	19,142

2.2 Methods

2.2.1 Deep Neural Network (DNN)

DNN is a series of algorithms designed to identify underlying relationships among dependent and independent variables by using a process that mimics the way the human brain operates. A generalised DNN procedure has the following five steps [90]:

1. coefficients (Θ) initialisation using Xavier approach [38]
2. forward propagation (obtaining a and z)
3. cost function (J) calculation
4. backward propagation (obtaining da, dz, and $d\Theta$)
5. coefficients update, then go back to step 2 until the cost function converged.

Initialisation and Forward Propagation

In this study, the algorithm (so called 'Xavier') of the first step is developed by Glorot and Bengio [38] and further proved by He et al. [45] that Xavier is one of the best initialisation methods for the training with a small number of inputs (i.e. less than 20). The equation is expressed as

$$\Theta^l = \frac{2}{p_{in} + p_{out}} \tag{2.2}$$

where p_{in} and p_{out} are the numbers of input and output units of the lth layer respectively. Θ^l is the coefficient set in the l layer in Fig. 2.2. The detailed structure of a DNN system is shown in Fig. 2.2 which describes the structure of the aforementioned three layers. From left to right are input, hidden and output layers respectively. It should be noted that more than one sublayer can exist in the hidden layer (larger than or equals to three). The equations in the figure describe how forward propagation works (the second step of neural network procedure). During the backward propagation (in this study, the mini-batch gradient descent [49, 87] is selected as a backward approach), Θ will be optimised together with the cost function J. x and $h_\theta(x)$ are the input and output of the model respectively. In addition, $g^{(l)}$ is the activation function for the lth layer, which is normally highly non-linearised, such as a rectified linear unit ($ReLU$), $Tanh$ and $Sigmoid$. Their equations are expressed as:

$$ReLU(x) = max(0,x) \tag{2.3}$$

$$Tanh(x) = \frac{e^x + e^{-x}}{e^x - e^{-x}} \tag{2.4}$$

$$Sigmoid(x) = \frac{1}{1 + e^{-x}} \tag{2.5}$$

L2-regularisation based DNN

One of the common problems for the traditional neural network is that it can be easily overfitted/underfitted [24], especially for the cases that have only one hidden layer. This issue is normally dealt with using regularisation algorithm [98], and in this study, one of the

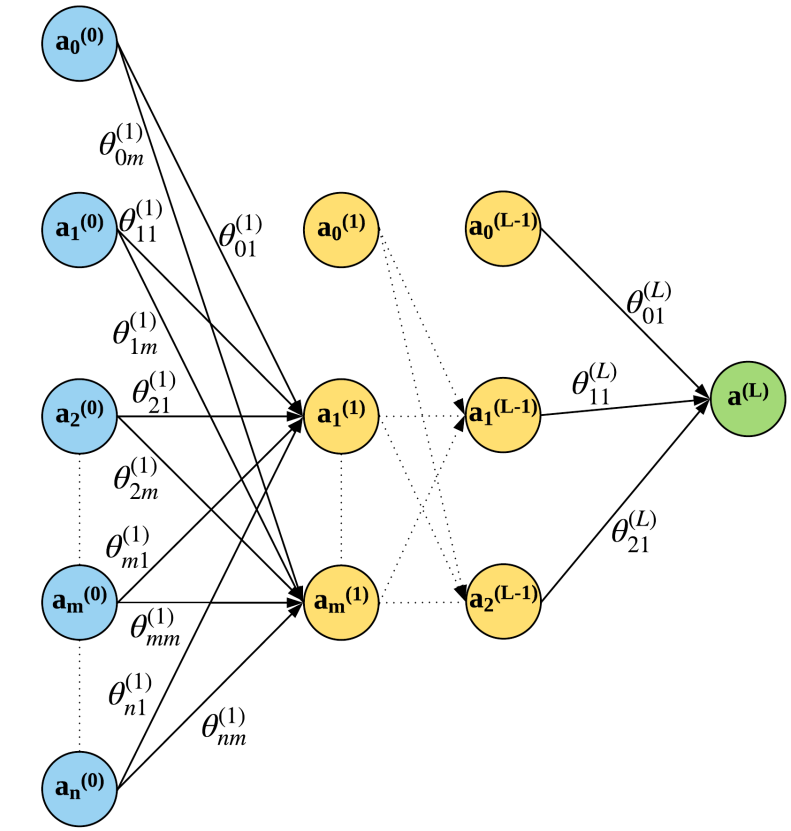

Fig. 2.2 Three layers of DNN: input (blue); hidden (yellow) and output (green) layers. 'a's are the values of each cell (the round boxes in figure). The superscript of 'a' represents the index of the layer and the subscript of 'a' represents the index of the cell in that specific layer. '$a_0^{(l)}$'s denote the bias units in each layer ('l' is the index of the layer). $\Theta^{(l)}$ is the cluster of all 'θ's on the linkage between the $(l-1)$th layer and the lth layer, and $\theta_{nm}^{(l)}$ means the coefficient between the nth cell in the $(l-1)$th layer and the mth cell in the lth layer. x and $h_\theta(x)$ are the input and output of the system respectively. In addition, $g^{(l)}$ is the activation function for the lth layer and $h_\theta(x)$ is the symbol for the whole DNN fitting model.

advanced algorithms — the L2 regularisation algorithm [75] is chosen for this purpose. The L2 cost function equation (i.e., general quadratic cost) of the bth cell in the lth layer can be expressed as (also the step 3 in the neural network procedure):

$$J^{(q)} = \underbrace{\frac{1}{2k}\sum_{i=1}^{k}\left(y^{(q)[i]} - h_{\theta}^{(q)[i]}(x)\right)^2}_{\text{regular J}} + \underbrace{\frac{1}{k}\frac{\lambda}{2}\sum(\theta^{(q)})^2}_{\text{L2 regularised cost } (J_{L2})} \tag{2.6}$$

where λ is the regularised factor and k is the number of training/sample data. y is the value of dependent variable (or measurement, i.e., N_e in this study) in the output layer, and it denotes the reference of each cell in each layer back-propagated from the measurement. q is the index of the outputs (in this study, q=1). It should be noted that, based on our experiments, L2-regularisation is better than the dropout approach (another commonly used advanced approach) in this case (not shown here).

In addition to the regular $d\Theta$, the gradient of L2 regularised cost function in backward propagation (as an extra component of the regularised $d\Theta$) is the same as Hu et al. [55]. So is the gradient descent procedure [55].

After regular training, the aforementioned dataset — cross-validation dataset is used to obtain the optimal λ. The flowchart for the overall L2 regularisation based DNN procedure is shown below. In addition, the network of the study has three hidden layers, the number of neural units in each layer is 16, 16, 8 respectively, and their activation functions are *Relu*, *Tanh* and *Sigmoid* respectively. This configuration is based on our historical experience considering both accuracy and efficiency.

2.2.2 Recurrent Neural Network (RNN)

Recurrent Neural Network (RNN) takes the sequential variation nature among sample data into consideration which is ignored by the ANN method. The structure of an RNN system is detailed in Fig. 2.4. In comparison with the ANN, temporary results from the current epoch will influence the model in the next epoch. X_t is the independent variable set at the tth epoch, and Y is the independent variable. h_t is the temporary results from the tth RNN unit, h_0 is manually initialised. The connection between h and Y are normal softmax/regression. Each RNN unit can be considered as an DNN model (Fig. 2.2). Ws and bs are the coefficients and biases that need to be estimated during the training. In addition, H is the *Tanh* function.

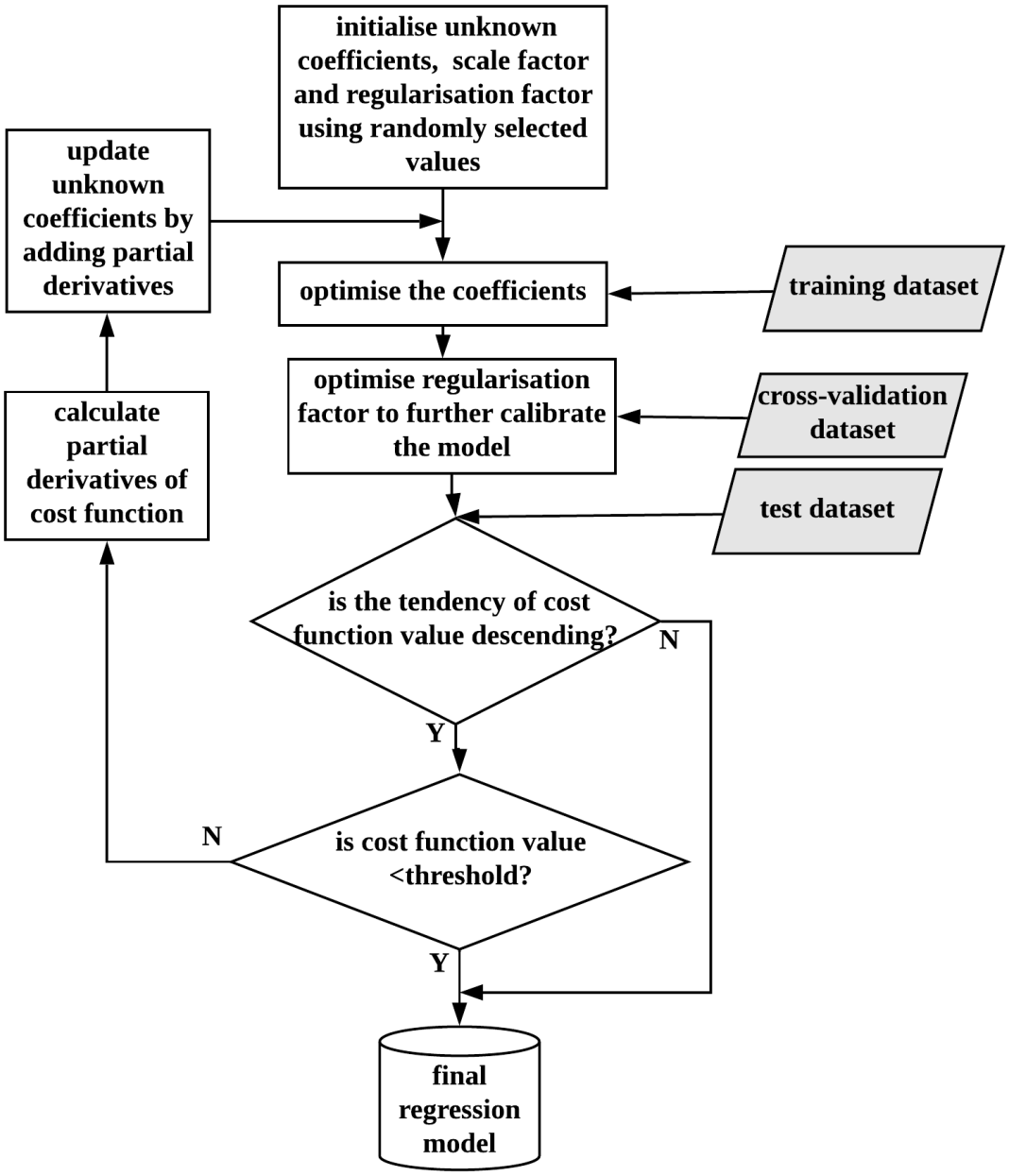

Fig. 2.3 Flowchart showing the process to obtain a regression model using DNN. The greyed parallelograms indicate the section of the dataset used at each stage in the process, white rectangles indicate the processes, white diamonds indicate the questions that control the following steps and the white cylinder is the final DNN derived model.

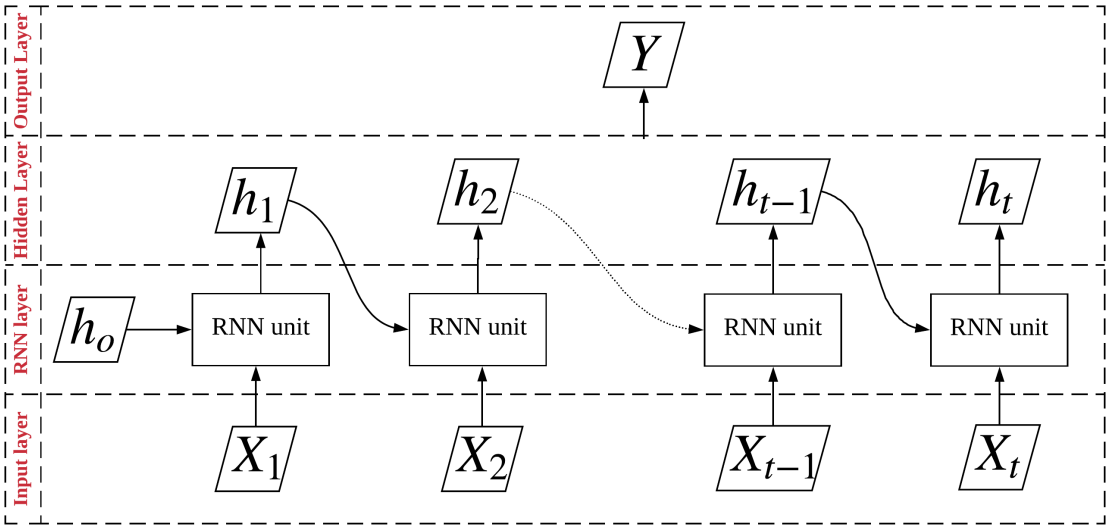

$$RNN\ unit: h_t = H(W_{xh}x_t + W_{hh}h_{t-1} + b_h)$$
$$output\ layer: Y = W_{hy}h_t + b_y$$

Fig. 2.4 Structure of RNN. X_t is the independent variable set at the tth epoch, and Y is the independent variable. h_t is the temporary results from the tth RNN unit, h_0 is manually initialised. The connection between h and Y are normal softmax/regression. Each RNN unit can be considered as an ANN model (Fig. 2.2). 'W's and 'b's are the coefficients and biases that need to be estimated during the training. In addition, H is the *Tanh* function.

Long Short-Term Memory (LSTM) Method

Currently, LSTM method is one of the most widely used RNN methods which inherits the advantages of RNN. In addition, the influence of sample data at a specific epoch to the traditional RNN unit will dwindle with the epoch going by. In order to investigate the feature of the temporal sequences, a new type of interim result — memory cell c is applied in LSTM as is shown in Fig. 2.5. c can keep the historical data in memory, and wake it up in any epoch when needed. The Input gate (i) and Forget gate(f) decide the relative weights of this RNN cell and historical memory cell respectively, and o is the output gate. The detailed algorithm is described in Fig. 2.5 as well.

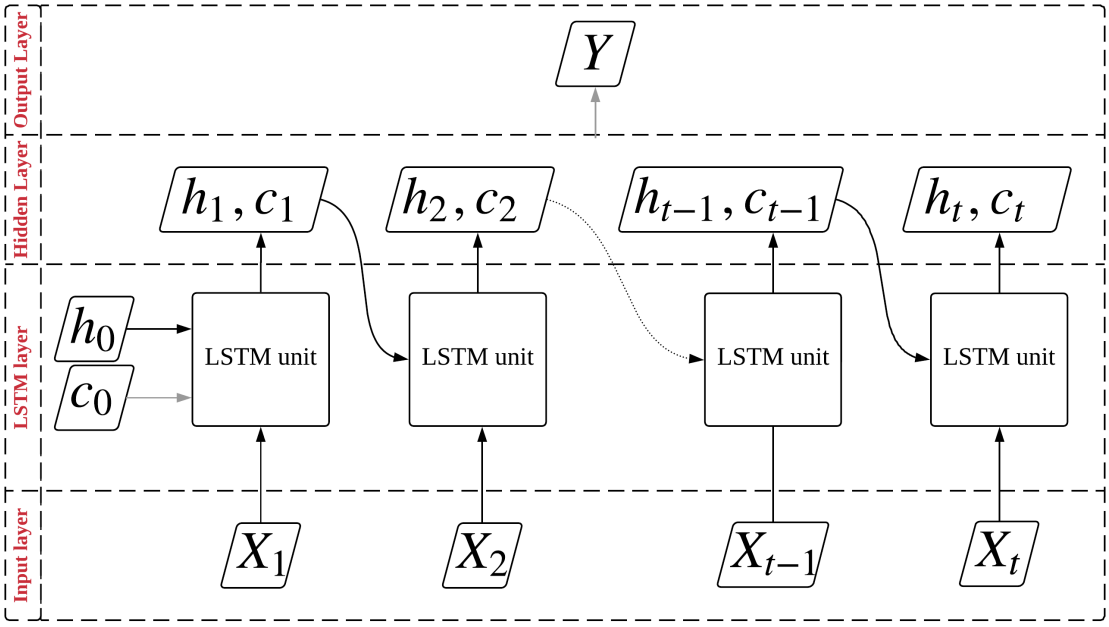

$$
\begin{aligned}
i_t &= \sigma(W_{ix}x_t + W_{ih}h_{t-1} + b_i) \\
f_t &= \sigma(W_{fx}x_t + W_{fh}h_{t-1} + b_f) \\
o_t &= \sigma(W_{ox}x_t + W_{oh}h_{t-1} + b_o) \\
c_t &= f_t c_{t-1} + i_t * tanh(W_{cx}x_t + W_{ch}h_{t-1} + b_c) \\
h_t &= o_t * tanh(c_t)
\end{aligned}
$$

Fig. 2.5 Structure of the LSTM. Similar to RNN (Fig 2.4) but with memory cell c added. i, f, o are the input gate, forget gate and output gate respectively. σ is the *Sigmoid* function.

Bidirectional LSTM (bi-LSTM) Method

Memory cells in LSTM can carry forward the information from previous sample sets into the prediction of Y ultimately. However, the implementation process is directional, forward-only, which ignores the backward connection and makes the model less robust. To solve this disadvantage, the training process in the Bi-LSTM method is conducted in a sequential order not only forward, but also backward. The details of the Bi-LSTM method are shown in Fig. 2.6.

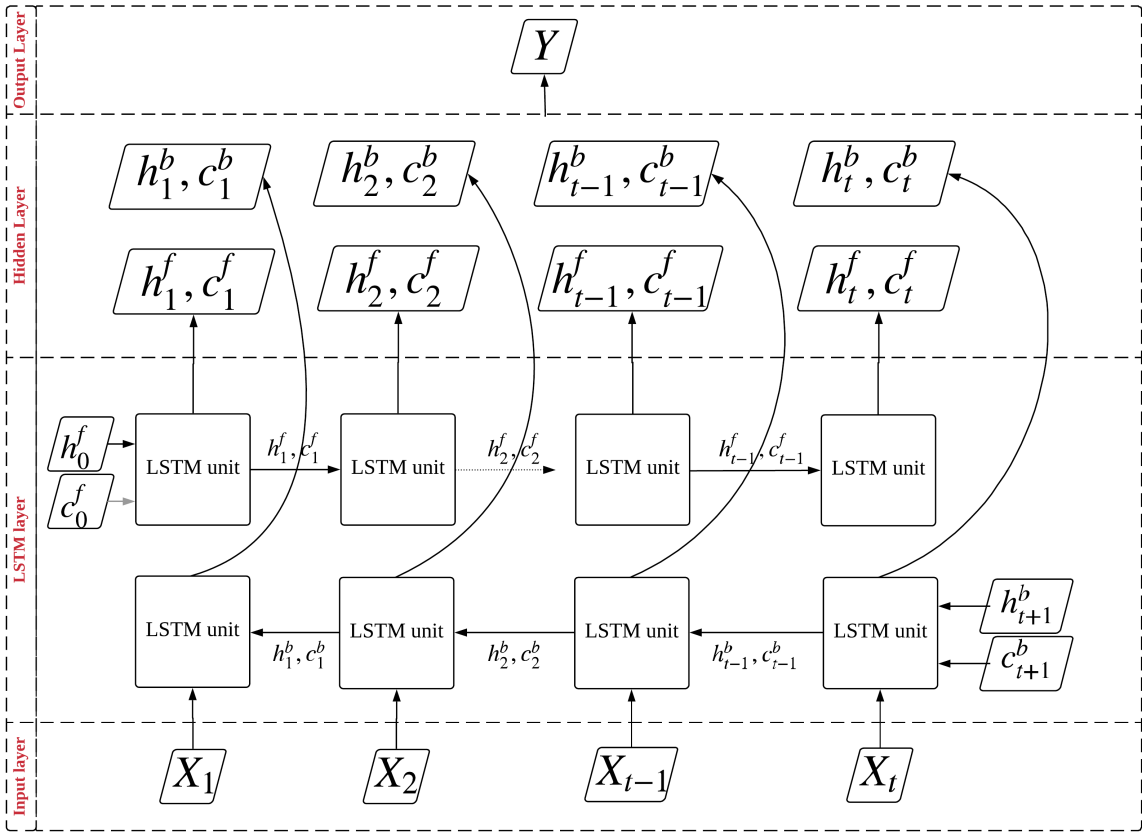

Sequential Forward

$$i_t = \sigma(W_{ix}x_t + W_{ih}h_{t-1} + b_i)$$
$$f_t = \sigma(W_{fx}x_t + W_{fh}h_{t-1} + b_f)$$
$$o_t = \sigma(W_{ox}x_t + W_{oh}h_{t-1} + b_o)$$
$$c_t = f_t c_{t-1} + i_t * tanh(W_{cx}x_t + W_{ch}h_{t-1} + b_c)$$
$$h_t = o_t * tanh(c_t)$$

Sequential Backward

$$i_t = \sigma(W_{ix}x_{t+1} + W_{ih}h_{t+1} + b_i)$$
$$f_t = \sigma(W_{fx}x_t + W_{fh}h_{t+1} + b_f)$$
$$o_t = \sigma(W_{ox}x_t + W_{oh}h_{t+1} + b_o)$$
$$c_t = f_t c_{t+1} + i_t * tanh(W_{cx}x_t + W_{ch}h_{t+1} + b_c)$$
$$h_t = o_t * tanh(c_t)$$

Fig. 2.6 Structure of the bi-LSTM method, similar to the LSTM method (Fig 2.5), the training is carried out in both directions (i.e. both sequential forward and sequential backward).

2.2.3 Helmert Variance Component Estimation Aided fast-Weighted Total Least Squares (Helmert-VCE-Aided fast-WTLS)

Helmert Variance Component Estimation Aided fast-Weighted Total Least Squares (Helmert-VCE-Aided WTLS) is an advanced least squares (LS) method. Compared with traditional LS, Helmert-VCE-aid WTLS method can not only automatically adjust the weight for each source of data for LS, but also mitigate the bias inside the design matrices. The details of this method are introduced in Chapter. 5.

2.3 Summary

This Chapter introduces the data and neural network methods used in this study in details. The data section includes the IGS, GNSS-RO, satellite altimetry, ionosonde and ISR data. The methods section includes DNN and RNN (including LSTM and bi-LSTM methods) and Helmert-VCE-aided fast-WTLS. They will be used in the the following sections.

Chapter 3

Topside Electron Density Modelling using DNN from GNSS RO Data

3.1 Introduction

Electron Density (N_e) is one of the most important ionospheric parameters that describes how many electrons in a unit volume (commonly in 1 m^3 or 1 cm^3) at a specific altitude. The variations and anomalies of N_e have been investigated by many researchers [3, 34, 102, 31, 69, 19, 95] since 1940s. Nowadays, with the development of GNSS, those N_e study becomes more and more important since dual-frequency GNSS positioning can only remove the first-order ionospheric delay, and higher-order ionospheric effects [52, 54] sometimes can be non-negligible especially during high ionospheric disturbance periods [80]. High-resolution vertical N_e profiles have been used widely in investigating those ionospheric anomalies (e.g., equatorial plasma bubble [31] and travelling ionospheric disturbances [102]).

A number of instruments are used to measure N_e profiles, and they can be broadly divided into two categories: ground-based (e.g., ISRs [62] and ionosondes [83, 62]) and satellite-based (e.g., Topside Sounder (TS) satellites [20, 9] and GNSS-RO satellites [92, 116, 97]). Currently, the most frequently used N_e data are measured by ionosonde which have been collected since the early 20th century. There are hundreds of ionosonde stations operating all over the globe, and each station can provide N_e measurements in 15-30 minutes interval. However, the flip side of the ionosonde measurements is that it cannot measure N_e profiles in the topside ionosphere (above the peak of the F2 layer (i.e., hmF2) in the ionosphere) which are very important in the ionospheric study. Topside information is currently obtained from model prediction [9] based on either bottomside measurements (e.g., Vary-Chap function [81] in the IRI) or physical mechanism (e.g., TIEGCM [67]). Topside information from both

methods is prone to the effect of inherent assumptions in the models which could lead to a potential bias problem in the prediction. The investigation of an enhanced topside model in both spatial and temporal domains from topside measurements is, therefore, significant for GNSS precise positioning and the study of the upper atmosphere.

Three of the aforementioned data sources (ISR, topside sounder and GNSS-RO) can provide the topside measurements. Although ISR by far is the most powerful ground-based remote-probing tool for the study of the ionospheric process [62], the horizontal coverage of ISR is too limited (the window of sky view over the ISR station is very small) to be adopted for global modelling. ISR data are thereby used as a reference in this study instead. In addition, topside sounder satellites are no longer operational and there have been no launches since the 1980s [9]. The horizontal distribution of measurements from topside sounder satellites is not as good as that of GNSS-RO. An analysis of GNSS-RO and ground-based data shows that COSMIC, which is one of the GNSS-RO missions, profiles are generally in a good agreement with ionosonde profiles both in NmF2, hmF2 and the bottomside part of the profiles [59]. The comparisons made between COSMIC derived N_e profiles and those measured by ISR at Millstone Hill in Massachusetts (mid-latitude) and Jicamarca (low-latitude) in Peru is shown by Lei et al. [64]. Generally, the COSMIC profiles agree well with the ISR measurements. Thus, GNSS-RO data are considered to be the optimal data source for the topside N_e modelling in this study.

As is mentioned above, generally there are two kinds of topside N_e (above hmF2) models —the empirical and physical models. In addition to the spatial and temporal features considered, the empirical topside model is mostly based on the characteristics of the topside profile [19, 9] (e.g., the Chapman model consists of the effective scale height [70]), and the physical/semi-physical model has taken some physical features (e.g., Kp, $F_{10.7}$ and magnetic fields) into account [82].

Due to the fact that the exact relationship between N_e and the independent variable set is unknown, DNN is used in this study. Again, the DNN was initially inspired by biological neural systems for regression or classification of an unknown function based on a large amount of input/training data. Nowadays, a neural network has been widely used in many fields, e.g. data mining [18], atmospheric modelling [101, 55, 45, 88], and even automatic driving [33]. It is well-known that a set of observation equations (or so-called “design matrices”) need to be designed first in the traditional Least Squares (LS) estimation method for regression modelling [74]. The design matrices are generally based on the assumed relationships between the dependent and the independent variables. However, as mentioned above, some of the exact relationships are unknown. Fortunately, neither the observation equations nor apriori knowledge of the relationship is required in the modelling of ANN.

This network system can automatically construct the optimal regression function based on the sample data and the designed network [43].

This study investigates a new four dimensional (in spatial and temporal domains) topside N_e model constructed from GNSS-RO measurements using a L2-DNN approach and a comprehensive independent variable set (which is so-called "training"), and then obtains the N_e (which is so-called "prediction") by giving the input set. However, several physical variables in the input set, representing the features of N_e profile (including electron density peak (NmF2) and hmF2), cannot be obtained everywhere (or anytime) without an external data source (e.g., models). Therefore, in this study, hmF2 and NmF2 models are developed from COSMIC (similar to the model developed by Sai Gowtam and Tulasi Ram [88]) for providing the inputs (subsequently used during the prediction) where hmF2 and NmF2 measurements are unavailable (hereinafter this scenario is called "with sub-models" mode). The same modelling approach is used in the construction process of the two sub-models. "Out-of-sample" COSMIC measurements (which are not used in model training process), together with the data from other GNSS-RO missions (e.g. GRACE) and ISR are used as references to evaluate the performance of the new N_e model. In addition, the effectiveness of each variable (including two sub-models) and the characteristics of the new model results, are also investigated.

3.2 Paper A: Four-dimensional Topside Electron Density Modelling using L2-ANN from GNSS-Ionospheric Radio Occultation Data

Citation: Hu, A.; Wu, S.; He, C.; & Zhang, K. Four-dimensional Topside Electron Density Modelling using L2-ANN from GNSS-Ionospheric Radio Occultation Data (Under Review)

Status: Submitted to Space Weather on 3 May 2019

3.3 Summary

In this study, a new topside four-dimensional N_e model was developed using an advanced deep-learning technique (L2-DNN) and the COSMIC satellite-to-satellite limb sounding (i.e. GNSS-RO) measurements. A new variable set by considering both physical and empirical information in the ionosphere was designed. Two sub-models (i.e. NmF2 and hmF2)

were developed and subsequently used as inputs in the DNN when no hmF2 and NmF2 measurements were available. The performance of the new model was then evaluated by comparing with IRI-2016 model using the out-of-sample COSMIC data as well as GRACE and ISR data as references. The effectiveness of each variable and modelling approach was also investigated and the results showed:

- Compared with the out-of-sample COSMIC measurements, hmF2 and NmF2 sub-models agree better than the international reference ionosphere-2016 (IRI-2016) by 4.5% and 11.0% respectively;
- The new model developed outperforms IRI-2016 by 35%, 36% and 53% in comparison with out-of-sample COSMIC, GRACE, and ISR data respectively. In addition, the model with sub-models also outperforms IRI by 16% with regards to ISR data;
- The spatial and temporal variables, together with hmF2, NmF2 and $F_{10.7}$, K_p affected the performance of the topside Ne model significantly.
- The new model inherited the characteristics of COSMIC measurements in low and high solar activity conditions. The EIA and MSNA phenomenons were also revealed in both the model outputs and COSMIC measurements;
- The new model agreed better with GRACE data rather than ISR (relative differences: 12.4% versus 24.3%), which may suggest that the quality of GRACE data are similar with that of COSMIC in this type of applications. Hence, GNSS-RO may be considered as a new and promising source of measurements in improving the performance of the topside N_e model in future.

Chapter 4

Investigation of Topside VSH Based on GNSS-RO Measurements

4.1 Introduction

The scale height is often used to characterise N_e profile [99, 4, 70]. Three definitions for scale height can be found in the literature —plasma scale height (H_p), effective scale height (H_m), and VSH [70]. H_p can be directly obtained from T_p using $H_p = k_b T_p / m_i g$. H_m is defined as the scale height of a Chapman-α function fitting the N_e profile taking both the topside and bottomside of the ionosphere into account. The VSH is generally defined as the value of $dh/d(ln(N_e))$, relating to the gradient of the topside N_e profile [61]. The relationship between the three scale heights has been explored [63, 42]. The VSH, as one type of ionospheric scale heights, has been used in ionosphere studies (e.g., geomagnetic storm analysis [42]). VSH, together with NmF2 (the peak electron density in the F layer) and hmF2 (the height of peak electron density), can be used to reconstruct topside electron density (N_e) profiles (especially below the transition height). Both NmF2 and hmF2 can be obtained from a classical empirical model, e.g. IRI model [14, 7, 8, 15, 11]. VSHs obtained from Topside Sounder (TS) measurements do not have sufficient density/coverage of observations in some regions. Establishing a global VSH model using homogeneous observations around the world is therefore important for the construction of global ionosphere models.

It is well known that the T_e, as the main component of T_p, strongly depends on the local slope of the vertical electron density profile [e.g., 16, 70]. There are no techniques that can provide long-term global T_e measurements with a high vertical resolution except empirical/physical models, it is important to adopt VSH as an independent variable to aid the model (such as T_e-N_e model). In addition to utilise VSH in modelling, although the

characteristics of topside ionosphere is too complex to be described only by VSH, VSH can still be used for the investigation of the complex topside ionosphere. For example, the constant Ne gradient assumed in the VSH definition implies a constant plasma temperature in O+ dominated topside ionosphere by neglecting the presence of He+ ions [61, 60].

The ionospheric VSH of an EDP is generally defined as the value of $dh/d(ln(Ne))$ from the topside EDP (from $1.1\times$hmF2 to max(hmF2+200,500) km, which is O+ predominance) [61]. More specifically, VSH is the first derivative of altitude (h) with respect to $ln(Ne)$ at the peak of EDP in F layer $(NmF2)$ [61, 60]. It should be noted that the correlation coefficient of VSH will be poorer if the upper boundary reaches the COSMIC's orbit. Traditionally, the VSH over a geographic location can be obtained from an EDP measured by instruments, such as TS, ISR and RO. If no such measurements are available, the only option is to use a global ionosphere model, such as the IRI or the TIEGCM model to obtain the VSH for a given location.

Depuev and Pulinets [30] developed a global topside EDP model by fitting the data from Intercosmos-19 topside sounders. Kutiev et al. [61] used 170,033 VSHs measured from two topside satellites—Aluoette and ISIS—and added extra variables (i.e. $F_{10.7}$ and K_p compared to Depuev and Pulinets [30]) to develop a new topside EDP fitting model. However, the variation of VSH with longitude has not been taken into consideration in their model, mainly due to the inhomogeneous distribution of the TS data with respect to longitude [61].

In addition, Gulyaeva [42] used TEC obtained from IGS GIM, together with the NmF2 and hmF2 obtained from ionosondes, as the input for IRI-Plas [8] to generate VSH. This research shows that the VSH increases with the absolute value of the geomagnetic latitude during a geomagnetic storm. However, in their study the conclusion was drawn using only the ionosonde data (i.e. the locations of seven ionosonde stations; five other stations were used for validation). Therefore, the horizontal resolution may not be adequate to reveal detailed global VSH features. A better VSH model based on new data sources is therefore required for obtaining a high spatial resolution of VSH values.

In this study, ionospheric RO data were used to investigate the inclusion of an additional variable – longitude– in the global VSH modelling process for improving the model accuracy. The quality of GNSS-RO data and its products has been assessed by many researchers. Lei et al. [64] showed some of the first comparisons made between COSMIC derived electron density profiles and those measured by ISRs at Millstone Hill in Massachusetts (mid-latitude) and Jicamarca (low-latitude) in Peru. Generally, the COSMIC profiles agree well with the ISR measurements. Lei et al. [64] and Stolle et al. [100] compared electron density profiles derived from RO measurements on-board CHAMP and COSMIC and ISR data. Generally speaking, the RO results agree quite well with ISR data on a comparison with F2 layer peak

density. Although RO data have been applied in the latest version of the IRI model (i.e. IRI-2016 [10]), this inclusion was limited to the hmF2. The data sources for the topside EDP modelling of IRI since IRI-2007 were from Aluoette and ISIS [15]. This analysis explores the possibility of incorporating RO data in the topside EDP modelling as a new source of data.

The traditional Base-Vector-Based Least Squares (BVBLS) estimation method [61] was used to estimate the unknown coefficients of a topside VSH regression model. In the event that longitude is added as a variable, the computational requirement is beyond the capacity of an ordinary PC or even a normal workstation. A more advanced and sophisticated technique – DNN – is proposed in this study to solve this problem and to explore the relationship between the VSH and longitude. The DNN is an effective tool in investigating if the correlation between a set of dependent variables and a new variable is significant.

In this study, a new VSH model is established from the COSMIC [91] measurements using the DNN approach. Its accuracy is assessed by comparing to models in various configurations with out-of-sample RO measurements and ISR measurements as internal and external references respectively. The effectiveness of each new variable is also assessed. In addition, the improvement of the VSH model in geomagnetic storm conditions is also explored.

4.2 Paper B: Modeling of Topside Ionospheric Vertical Scale Height Based on Ionospheric Radio Occultation Measurements

Citation: Hu, A., Carter, B., Julie, C., Norman, R., & Zhang, K. (2019). Modeling of Topside Ionospheric Vertical Scale Height Based on Ionospheric Radio Occultation Measurements. Journal of Geophysical Research:Space Physics, 124(6), 4926-4942. 10.1029/2018JA026280

Status: Published on 30 May 2019 in Journal of Geophysical Research:Space Physics

4.3 Summary

In the past, global VSHs were modelled using TS measurements and the BVBLS estimation method, and several spatial and temporal variables were included in the models. Longitude is usually excluded from the variable set of the modelling. One possibility is due to the inhomogeneous distribution of TS data along the longitudinal dimension and the limitation

of BVBLS on computational capacity. In this study, the DNN method was applied to global VSH modelling process to address the computational limitations of BVBLS. A new data source –RO data –was also used in the modelling. Since RO data are typically homogeneously distributed over the globe, it is possible to take the longitude into account in the variable set of the new model. Testing results showed that with the inclusion of longitude, the accuracy of the model improved by only around 1% globally, but was shown to have a substantial positive impact in equatorial and high-latitude regions. Further, the accuracy of the RO-derived models was found to be around 9% better than that of TS-derived models.

In terms of modelling techniques, this study revealed a couple of key advantages in adopting the DNN method for modelling the VSH over the previous BVBLS method. First, the VSH results from the DNN model were found to agree more closely than the BVBLS model with both the out-of-sample data and the independent ISR data from low, mid and high latitudes. Second, the DNN VSH results reveal a clear equatorial peak during the geomagnetic activity, which was not presented in the BVBLS results; the storm-time equatorial peak was verified in the RO observations.

In conclusion, it is suggested that the proposed VSH model could be used to update or improve the current empirical VSH models (even for T_e modelling in Chapter 7) and enhance the understanding of topside ionosphere.

Chapter 5

A New GIM Developed by Helmert-VCE-Aided fast-WTLS Method from Multi-Source of Data

5.1 Introduction

The ionospheric delay is proportional to the TEC along the ray path and inversely proportional to the frequency of the signal squared. It is one of the major errors in GNSS measurements, which significantly affects the performance of GNSS applications such as single-frequency positioning. If this delay can be accurately estimated, the ionospheric error in GNSS measurements can be corrected or considerably mitigated. Since the ionosphere is a dispersive medium, the ionospheric delay can be largely mitigated using the differential approach – a linear ionosphere-free combination of simultaneous dual-frequency GNSS measurements. However, for single-frequency measurements, the ionospheric delay cannot be mitigated through the differential approach. In this case, an ionospheric model can be used to correct the ionospheric delay at the user's location. The ionospheric model can be derived from a network of GNSS reference stations where dual-frequency receivers are deployed. The vertical TEC (VTEC) values over all the network stations are often used to develop a VTEC model for the region covered [57].

Several types of global empirical VTEC models have been developed, e.g. the Global Assimilative Ionospheric Model [26, 27], and empirical models such as NeQuick [50, 82] and the IRI [14, 7, 8, 15, 11, 10]. In addition, several different GIMs are produced by a number of IGS data processing centres [84, 115, 112], including NASA JPL, European Space Agency (ESA), the Polytechnic University of Catalonia (UPC), Center for Orbit Determination in

Europe (CODE) etc. All of these are official near real-time ionospheric products of the IGS Ionosphere Working Group using a similar approach (i.e. spherical harmonic (SH) models with a 2-hour temporal resolution). Detailed comparison among the current GIMs can be found in Hernández Pajares et al. [48].

Traditional VTEC data used for producing GIMs are obtained from ground-based GNSS measurements collected at global IGS stations. In a 2-hour period, the number of measurements can reach one million, which is regarded to be sufficient for generating a high-accuracy GIM [46, 47, 73]. [66] estimated GIMs by an innovative approach –SHPTS functions and the data from the BeiDou-2 system were also used in the modelling. However, due to the lack (or low number) of IGS stations in some regions, especially over the oceans, the GIMs produced may not perform well across the entire globe.

In order to improve the performance of GIMs, Todorova et al. [104] established another GIM by incorporating VTECs derived from GNSS measurements with satellite altimetry (e.g. Jason-1) measurements mainly for compensating insufficient data over the oceans. The performance of the GIMs showed significant improvements, but the inhomogeneous distribution of the satellite altimetry data over the oceans is still a factor limiting the model's performance. To overcome this problem, Alizadeh et al. [1] for the first time took into consideration an additional data source – VTECs retrieved from GNSS-RO of the COSMIC/FORMOSAT-3 satellites into global ionospheric modelling and the accuracy of the VTEC GIM over the ocean regions was further improved. The combined GIMs of VTEC show a maximum difference of 1.3–1.7 TECU with respect to the GNSS-only GIMs on the whole day.

When the VTEC data used in the LS estimation for the optimal coefficient estimates of the ionospheric model have different precision or qualities, the use of appropriate weights plays an important role in getting the "optimal" estimates. Therefore, instead of using the apriori variance (or covariance) of the observations to determine the weights, Chen et al. [27] applied a Helmert VCE method to estimate the variance of each type of observations, and the results showed further improvement to the GIMs [27].

In addition, each element in the design matrix of the observation equations is usually a fixed value derived from the approximate coordinates of the ionospheric pierce point (IPP) for each of the VTECs derived from ground-based GNSS and Jason observations. However, for each RO-derived VTEC, the coordinates for the tangent point (similar to the IPP for a GNSS observation) of the RO event vary during the event which can last 1-2 minutes, thus its coordinates are no longer fixed values (up to 10 degrees in the geomagnetic coordinate frame). This means that neglecting the uncertainty in the elements of the design matrix may not be appropriate. In this study, the fast WTLS method was adopted [39, 89, 94] instead of using the conventional least squares estimation and the uncertainty of the elements in

the design matrix was also taken into account in this approach. Moreover, the sequential technique was also used (rather than the conventional batch processing approach) in order to reduce the large computational load of the model estimation process.

In order to assess the improvement of the new approach, the latest GIM developed by the GIPP of the Chinese Academy of Sciences (hereinafter called 'CAS') [66, 114]. The CAS model was based on SHPTS and validated using several data sources. This includes the ionospheric TECs retrieved from global GPS data, the GIMs released by the other Ionospheric Associate Analysis Centers (IAACs), the TOPEX/Poseidon satellite and the DORIS etc. According to Li et al. [66], the CAS model could achieve an accuracy of 2–6 TECU approximately over areas without GNSS observations, and its performance is similar to those of other models released by IAACs. To further validate the accuracy of the new model, out-of-sample Jason-3 measurements are also used as an external reference in this study.

5.2 Paper C: Helmert-VCE-Aided fast-WTLS Approach for Global Ionospheric VTEC Modelling Using Data from GNSS, Satellite Altimetry and Radio Occultation

Citation: Hu, A., Li, Z., Carter, B., Wu, S., Wang, X., Norman, R., & Zhang, K. (2019). Helmert-VCE-aided fast-WTLS approach for global ionospheric VTEC modelling using data from GNSS, satellite altimetry and radio occultation. Journal of Geodesy, 93(6), 877-888. DOI: 10.1007/s00190-018-1210-7

Status: Published on 14 November 2018 in Journal of Geodesy

5.3 Summary

In this study, an innovative approach –Helmert-aided fast-WTLS was proposed to enhance global VTEC modelling process. Three VTEC data sources including ground-based GNSS, satellite altimetry and RO data were used to establish a global SH model for generating a GIM. Test results showed: 1) the fast-WTLS approach can improve the accuracy of the GIMs by around 5% since the uncertainty of the design matrix of the observation equations of the SH model has been taken into account; 2) the accuracy improvement was more pronounced when the GIMs (provided by GIPP, i.e. CAS) was selected as the reference (roughly 8%); and

3) the improvement of the proposed model over the ocean is validated by using out-of-sample Jason-3 measurements as reference and about 20% improvement (mostly over the ocean) has been achieved.

Chapter 6

Using Bi-LSTM Method for hmF2 Forecasting from Ionosonde Measurements in Australian Region

6.1 Introduction

The height of F2 peak (hmF2) is an essential ionospheric parameter that is defined by the altitude of N_e peak in the ionosphere. The variation of the hmF2 reflects the ionospheric variability. Therefore, it can also reveal the activity of either the earth magnetic field (B) or the solar wind [76, 40]. In addition, hmF2 forecasting can be considerably important in analysing the structure of ionosphere and enhancing both GNSS positioning and LEO orbit determination (especially during scintillation) capabilities.

The hmF2 can be obtained through a number of techniques, such as digisondes/ionosondes, GNSS RO satellites and topside sounders. Ionosonde is a typical ionospheric sounding device that has been used widely for over 90 years (can be traced back to 1920s [29]) due to its high accuracy. Currently, there are hundreds of ionosonde stations operating all over the globe, and each station can provide hmF2 in 30 minutes frequency. Therefore, ionosonde-derived hmF2 has been widely used as the data source for ionosphere modelling (e.g., IRI [12, 13, 15, 71, 2, 11, 10]). The ionosonde-only model developed by Altadill et al. [2]. is called the "AMTB" model which represents the first character of the four authors' surnames. Concurrently, Hoque and Jakowski [51] established their model based on data from both the ionosonde measurements and GNSS-RO, including CHAMP, GRACE, and COSMIC. Shubin et al. [96] developed a hmF2 model based on radio occultation data from COSMIC,

GRACE, and CHAMP only. The AMTB and Shubin's models have been selected for the inclusion in the 2016 version (the latest version) of the IRI model [10].

Sai Gowtam and Tulasi Ram [88] carried out the hmF2 modelling in a different way. Most current models are established using known base functions (i.e. empirical orthogonal functions or spherical harmonics functions) which may not be perfect. Sai used the ANN technique (with only one hidden layer) to estimate the coefficients without knowing the base function of independent variables in advance from COSMIC (*ibid*). Tulasi Ram et al. [109] then further enhanced his model by including other RO measurements (i.e. GRACE and CHAMP) as well as ionosonde data as data sources. Furthermore, he also assessed the performance of the ANN model by comparing with IRI-2016 model, and also proved that the anomalies of ionosphere (e.g., EIA and MSNA) are well captured by the model [88, 109].

All the above models, however, have a common disadvantage that several physical parameters, such as $F_{10.7}$ (a measure of solar flux per unit at a wavelength of 10.7cm) and K_p (a global geomagnetic activity index) which can only be measured in real-time (or near-real-time) are required as inputs for the hmF2 models. Therefore, the values of those physical parameters have to be estimated during the process of hmF2 forecasting which may impact the quality of the hmF2 output from the model.

In this study, a more advanced machine learning technique —bidirectional Long Short-Term Memory network (hereinafter termed "bi-LSTM" [93]) is used for predicting/forecasting hmF2 from ionosonde-only data at 12 ionosonde stations in the Australia region. In comparison with ANN, the Bi-LSTM method can be considered as a special type of the RNN technique which takes into account of the sequential variation of hmF2 value. This advantage offers us an opportunity to perform the prediction by using the data in recent epochs. However, this technique has some disadvantages. The most important one is that the sample data of the model must be continuous (each sample set must have the same time intervals) and at the same location, which is not as flexible as ANN. This is another reason why the ionosonde data were selected for this study (i.e. continuous measurements at a fixed location). First, hmF2 models for each station were established and assessed, then a regional hmF2 model was built by considering the geographic location of the stations (i.e. longitude and latitude). The three models aforementioned, i.e. AMTB, Shubin and ANN models [90] were selected for comparison. The traditional LSTM model was used for the evaluation to show the advantages of the bi-LSTM. Out-of-sample ionosonde data were used as the reference.

6.2 Paper D: Using Bidirectional Long Short-Term Memory Method for the Height of F2 Peak Forecasting from Ionosonde Measurements in the Australian Region

Citation: Hu, A., & Zhang, K. (2018). Using Bidirectional Long Short-Term Memory Method for the Height of F2 Peak Forecasting from Ionosonde Measurements in the Australian Region. Remote Sensing, 10(10), 1658. DOI: 10.3390/rs10101658

Status: Published on 10 October 2018 in Remote Sensing

6.3 Summary

In this study, a new Australian regional hmF2 forecast model was developed from ionosonde data using the Bi-LSTM method. With this new model, hmF2 values can be predicted well forward up to five hours using the data in the past five hours. Decimal Month, LT, geographic longitude and latitude, together with K_p, $F_{10.7}$ and hmF2, in the past five hours, were chosen as an independent variable set to model the hmF2 in the hour forward. Various assessments have been conducted by comparing the new model with the AMTB, Shubin, ANN and LSTM models. Results showed that:

1. The new bi-LSTM and LSTM models substantially outperform the other three tested models, even when real-time data are used as part of the input for these three models.

2. The new model is more robust, and more easily and rapidly converge compared to the LSTM model. The overall performance improvement of the new bi-LSTM model is 30% compared to the ANN regional model.

3. The minimum sample numbers for the LSTM and bi-LSTM methods to converge are around 3000 and 2000 respectively.

4. The biLSTM-1h and biLSTM-3h (using the bi-LSTM for predicting hmF2 in 1, 3 and 5 hours forward at each station) agree better with ionosonde measurements compared to the Shubin model, but the biLSTM-5h is slightly worse than that of the Shubin model.

5. The performance of the Shubin model is better than that of the AMTB model in Australian region.

Chapter 7

Global Topside Electron Temperature Modelling from ISR Measurements

7.1 Introduction

Ionospheric plasma temperature (T_p) reflects the overall energy absorbed from solar and cosmic radiation by the upper atmosphere and is one of the essential factors reflecting the ionospheric variability [103]. It is also found that the variation of T_p affects the thermal equilibrium in the Earth's upper atmosphere significantly [120]. T_p is taken to be the average of ion temperature (T_i) and electron temperature (T_e). The value and variation of T_e are considerably larger than those of T_i, especially in the topside ionosphere. Hence, T_e variation (in both spatial and temporal domains) is the primary research focus of this study. Obtaining a high-resolution high-quality T_e map all over the globe could prove to be significant for gaining a better understanding of the upper atmosphere and its interaction with the space environment.

T_e is measured by various instruments (e.g., incoherent scatter radar (ISR) station from the ground, and ISIS, AE-C and AEROS satellites from the space). However, none of them can provide T_e measurements with both high spatial and temporal resolution. Among all types of T_e measurements, ISR measurements have the best vertical resolution and accuracy [41, 32, 122, 58, 119, 63]. However, the disadvantage of ISR is that although a number of ISR stations are deployed all over the globe, only some of them can provide T_e measurements and the horizontal coverage of ISR is quite limited (the window of sky view over the ISR station is very small). In contrast, measurements from spacecrafts have better horizontal coverage but its vertical coverage and accuracy are not as good as that of ISR measurements. Hence, many efforts have been made to develop a T_e model in order to provide the global

T_e information with high quality and high resolution. Brace and Theis [16] used T_e and N_e samples from Atmosphere Explorer-C (AE-C) data during solar minimum to develop the Brace-78 model based on the relationship between T_e and N_e. Brace-78 still exists in the latest IRI model, although several essential factors such as solar activity (i.e. $F_{10.7}$), local time, season and magnetic condition (i.e. Kp/Ap) were not taken into account. Considering the sparseness of T_e and N_e data from one single spacecraft in both the spatial and temporal domains, Brace and Theis [17] used the data from multi-satellite missions (i.e. AE-C and ISIS-1/2) to develop four fitting models for T_e at 300, 400, 1400 and 3000 km altitudes with 8th order Legendre polynomials. The variables of the models were dip latitude, local time, solar activity, and magnetic activity. However, the T_e models exhibited a low vertical resolution, and N_e information was not considered in their study. Since then, many efforts have been made to improve Brace's models, e.g. Mahajan and Pandey [72], Bilitza and Hoegy [12], Titheridge [103], Truhlík et al. [107], Webb and Essex [110], Truhlik et al. [105, 106]. The TBT-2012 model developed by Truhlik et al. [106] is the latest T_e model and is applied in the IRI-2016 model. The TBT-2012 model used the variables of magnetic local time, invdip (calculated from invariant latitude and diplat) [108] and $PF_{10.7}$ (for solar activity). However, geomagnetic activity and N_e information have not been considered in these models accordingly, although it was shown that T_e significantly varies with N_e [63, 120, 16].

Instead of using traditional modelling approaches, the DNN, as an advanced artificial neural network technique is selected as the modelling method in this study due to the fact that the exact relationship between T_e and the whole variable set is not entirely known. The DNN technique has been widely applied in many fields, e.g. data mining [18], atmospheric weather prediction [101] and even automatic driving [33], since it is much more adaptive than many other machine learning methods (e.g., support vector machine) in regression modelling. More importantly, DNN is able to optimise the regression model without knowing the exact base vector of each independent variable, which makes it a powerful tool for space physics modelling.

In this study, both DNN and ISR data are used to model the topside T_e, and the N_e profiles, along with other variables such as VSH obtained from the topside N_e profile, are adopted as independent variables for this new T_e model. VSH is often used to characterise the topside of an N_e profile [99, 4, 70], which is generally defined as the value of $dh/d(ln(N_e))$, relating to the gradient of the topside N_e profile [61]. Lei et al. [63] showed evidence of the statistically relationship between the VSH and T_e profile in the topside ionosphere. Therefore, in this study, four variables reflecting the characteristics of the N_e profile (VSH, together with $hmF2$, $NmF2$ and correlation coefficient (r) between the measured N_e profile and its fitting profile (i.e., exponential function)) are added into the independent variable set of the new T_e model.

7.2 Paper E: A Deep Neural Network Model of Global Topside Electron Temperature Modeling Using Incoherent Scatter Radars and Its Application to GNSS Radio Occultation

Citation: Hu, A., Carter, B., Julie, C., Norman, R., & Zhang, K. A Deep Neural Network Model of Global Topside Electron Temperature Modeling Using Incoherent Scatter Radars and Its Application to GNSS Radio Occultation. (Under Review)

Status: Submitted to Journal of Geophysical Research: Space Physics on 7 August, 2019

7.3 Summary

In this study, the DNN technique was used to model the global topside T_e using ISR measurements, and out-of-sample ISR measurements were used to evaluate its performance. The model was also compared with the Brace-78 and TBT-2012 models. After obtaining the new model, T_e results can be generated from GNSS-RO measurements based on the new model and the results were then compared with T_e from TIEGCM to further investigate if the T_e variability was well captured by the new model.

In terms of modelling techniques, this study revealed a couple of key advantages in adopting the DNN method and ISR measurements for modelling the T_e over the existing methods. First, the T_e results from the new model were found to agree more closely than the Brace-78 and TBT-2012 models with the out-of-sample independent ISR data from low, mid and high latitudes. Second, the regional new T_e models can be converged by only taking 500 ISR profiles as modelling sample data and the accuracy of the model was shown to be improved by taking candidate variables into account during the DNN training. Eventually, the characteristics revealed by the DNN T_e results agreed with TIEGCM, e.g., the clear morning and evening enhancements in the altitude-LT and latitude-LT analysis. Furthermore, the study also proved that the bias between the new model and TIEGCM was mostly because TIEGCM always underestimates the N_e measurements.

One of the current limitations of this study is the inhomogeneous temporal distribution of observations from both ISR and RO which leads to the performance of the model during nighttime is not as good as that during daytime. Another limitation is the complex interactions in high-latitude region between the magnetosphere and ionosphere which result in a lower

reliability and accuracy of the high-latitude sub-model (existed in TBT-2012 and Brace-78 as well).

More and more GNSS-RO satellite missions are launched or being launched recently (e.g. COSMIC-2, FY-3E, etc), thus the number of RO data will be increased and the number of T_e profiles obtained from our model will be increase simultaneously. Besides, an advanced high-power phased array incoherent scatter radar is under construction in Sanya, China [121] which might be able to provide better data (especially in equatorial region) for the new T_e modelling in the near future. In conclusion, it is suggested that the proposed T_e model could be used to update or improve the current empirical T_e models (even for T_e modelling in future) and enhance the understanding of the topside ionosphere.

Chapter 8

Summary, Conclusion and Recommendation

8.1 Summary and Conclusion

The primary aim of this research was to investigate the application of the neural networks (including DNN and Bi-LSTM) and some other new methods (Helmert-VCE and WTLS) to develop new ionospheric models (including $hmF2$, electron density, electron temperature VSH and $VTEC$) based on multi-source data. The findings from this research suggested that the new techniques (especially the NN) have great potential to be used in ionospheric modelling. These new models developed are expected to be helpful in the application of GNSS positioning and space weather analyses. The main research tasks conducted and findings from the results are listed as follows:

- The Helmert-WTLS developed VTEC GIMs (with a 2h temporal resolution) can improve the determination of VTEC by 0.28 TECU over those from the Helmert-WLS approach (with reference to CAS) and by 1.61 TECU better than those from WLS, in terms of the mean RMSE in the 8-day testing period. In addition, by comparing with the out-of-sample Jason-3 observations, results from the proposed method also outperform Helmert-WLS, CAS and CODE models by 1.5, 2.4 and 2.4 TECU, respectively.

- The median of the relative residuals of the new VSH model is 8.5% less than that of the traditional approach/model (which was based on the TS data). The apparent errors in the polar region are mitigated by taking the variable longitude into consideration. The new model also agrees better than IRI model by around 14% and 10% with regards to the out-of-sample COSMIC data and ISR data respectively; In addition, the

characteristics of the global VSHs generated from the new model during geomagnetic storms agree with the reality better than that of the traditional model.

- The new T_e model has a relative error of 7.3% in the low-latitude region (i.e., against Arecibo data), 8.2% in the mid-latitude region (i.e., against Millstone Hill data) and 13.6% in the high-latitude region (i.e., against Poker Flat data), and all of them outperform IRI significantly. In addition, statistical analyses of the diurnal electron temperature profiles obtained from GNSS-RO show a good agreement with the TIEGCM outputs on some features.

- The new $hmF2$ model using Bi-LSTM can substantially outperform the current model (Shubin & AMTB) and those models using ANN and LSTM. Compared to the model developed by LSTM, the new hmF2 model is proven to be more robust and can rapidly converge. The minimum sample number required for the Bi-LSTM method (i.e. 2000) to converge is about 50% less than that is required for the LSTM method (i.e. 3000). In addition, compared to the Shubin model, the Bi-LSTM method can effectively forecast the hmF2 values up to 5 hours.

- The new topside N_e model developed agrees better than IRI-2016 by 35%, 36% and 53% with regards to out-of-sample COSMIC, GRACE, and ISR data respectively. In addition, the model developed with sub-models is also better than IRI by 16% with regards to ISR data. The spatial and temporal variables affect the performance of the topside N_e model significantly. In comparison with these variables, $F_{10.7}$ and K_p, together with $hmF2$ and $NmF2$, affect the performance on a smaller scale. The two sub-models ($NmF2$ and $hmF2$) agree better with the out-of-sample COSMIC measurements than IRI-2016 by 4.5% and 11.0% respectively. The new topside N_e model agrees well with COSMIC measurements during both solar maximum and solar minimum conditions. The ionospheric anomalies (e.g., MSNA and EIA) can be well captured by the new topside N_e model.

8.2 Future work

In the current study, most of the ionospheric models are used for nowcast (except hmF2 model) since either it is a short-term model or some real-time physical parameters are required as part of the input (e.g., k_p or $F_{10.7}$). $hmF2$ model can only forecast with the data from the past five hours at a specific geographic location. In addition, the DNN method is indeed a general universal method but it also results in the fact that DNN does not perform very well

in dealing with the dataset in either spatial or temporal domains. Both CNN and RNN are designed only for individual spatial and temporal dataset respectively, thereby they don't perform well in the spatio-temporal modelling. Fortunately, with the rapid development of modelling methods, some machine learning algorithms which perform well in both domains (e.g., Multi-Layer Recurrent Neural Network or Convolutional Recurrent Neural Network) are developed/matured, a forecast model with less limitation in both spatial and temporal domains is feasible. Hence, one future work is to investigate these advanced neural network methods and utilise them for advanced ionospheric modelling in order to not just improve the performance of the models but to show better physical features (namely, better fitting to the real ionosphere).

Although the NN used in this study is better than the traditional least-squares method in many areas, the uncertainties/covariance of coefficients are still missing (which do exist in the LS procedures). The uncertainties are pretty essential to help us understand not only what happens inside the model during the modelling, but also a physical mechanism explanation of the model. That is also one of the main reasons why so many space weather physicists are sceptical to machine learning. It is currently one of the top priorities in this area and also one of my primary research foci in future. I have tried to use several other machine learning techniques (e.g. Gaussian Process) to assist the NN in order to gain that uncertainty. Some achievements have been obtained and presented in a conference paper (i.e., IGL-1). Further publications are under preparation.

Nowadays, more and more GNSS RO satellite missions are either planned to be ready to launch, thus the number of RO profiles will increase significantly. An advanced high-power phased array incoherent scatter radar is under construction in Sanya of China which might be able to provide better data source (especially in the equatorial region) for the new T_e model [121] in the near future. Another future work will be focused on improving the quality and spatial resolution of the ionospheric model by assimilating new sources of data.

References

[1] Alizadeh, M., Schuh, H., Todorova, S., and Schmidt, M. (2011). Global ionosphere maps of VTEC from GNSS, satellite altimetry, and Formosat-3/COSMIC data. *Journal of Geodesy*, 85(12):975–987.

[2] Altadill, D., Magdaleno, S., Torta, J., and Blanch, E. (2013). Global empirical models of the density peak height and of the equivalent scale height for quiet conditions. *Advances in Space Research*, 52(10):1756–1769.

[3] Appleton, E. V. (1946). Two anomalies in the ionosphere. *Nature*, 157(3995):691.

[4] Belehaki, A., Marinov, P., Kutiev, I., Jakowski, N., and Stankov, S. (2006). Comparison of the topside ionosphere scale height determined by topside sounders model and bottomside digisonde profiles. *Advances in Space Research*, 37(5):963–966.

[5] Beutler, G., Rothacher, M., Schaer, S., Springer, T., Kouba, J., and Neilan, R. (1999). The international gps service (igs): an interdisciplinary service in support of earth sciences. *Advances in Space Research*, 23(4):631–653.

[6] Beyerle, G., Schmidt, T., Michalak, G., Heise, S., Wickert, J., and Reigber, C. (2005). GPS radio occultation with GRACE: Atmospheric profiling utilizing the zero difference technique. *Geophysical Research Letters*, 32(L13806).

[7] Bilitza, D. (1997). International reference ionosphere-status 1995/96. *Advances in Space Research*, 20(9):1751–1754.

[8] Bilitza, D. (2001). International Reference Ionosphere 2000. *Radio Science*, 36(2):261–275.

[9] Bilitza, D. (2004). A correction for the IRI topside electron density model based on Alouette/ISIS topside sounder data. *Advances in Space Research*, 33(6):838–843.

[10] Bilitza, D., Altadill, D., Truhlik, V., Shubin, V., Galkin, I., Reinisch, B., and Huang, X. (2017). International Reference Ionosphere 2016: From ionospheric climate to real-time weather predictions. *Space Weather*, 15(2):418–429.

[11] Bilitza, D., Altadill, D., Zhang, Y., Mertens, C., Truhlik, V., Richards, P., McKinnell, L.-A., and Reinisch, B. (2014). The International Reference Ionosphere 2012–a model of international collaboration. *Journal of Space Weather and Space Climate*, 4:A07.

[12] Bilitza, D. and Hoegy, W. (1990). Solar activity variation of ionospheric plasma temperatures. *Advances in space research*, 10(8):81–90.

[13] Bilitza, D., Huang, X., Reinisch, B. W., Benson, R. F., Hills, H. K., and Schar, W. B. (2004). Topside ionogram scaler with true height algorithm (topist): automated processing of isis topside ionograms. *Radio Science*, 39(1).

[14] Bilitza, D., Rawer, K., Bossy, L., Kutiev, I., Oyama, K.-I., Leitinger, R., and Kazimirovsky, E. (1990). International Reference Ionosphere 1990. *Tech. Rep. NSSDC/WDC-A-R and S*, 90(22).

[15] Bilitza, D. and Reinisch, B. W. (2008). International Reference Ionosphere 2007: improvements and new parameters. *Advances in space research*, 42(4):599–609.

[16] Brace, L. and Theis, R. (1978). An empirical model of the interrelationship of electron temperature and density in the daytime thermosphere at solar minimum. *Geophysical Research Letters*, 5(4):275–278.

[17] Brace, L. and Theis, R. (1981). Global empirical models of ionospheric electron temperature in the upper F-region and plasmasphere based on in situ measurements from the Atmosphere Explorer-C, ISIS-1 and ISIS-2 satellites. *Journal of Atmospheric and Terrestrial Physics*, 43(12):1317–1343.

[18] Brameier, M. and Banzhaf, W. (2001). A comparison of linear genetic programming and neural networks in medical data mining. *IEEE Transactions on Evolutionary Computation*, 5(1):17–26.

[19] Burns, A., Solomon, S., Wang, W., Qian, L., Zhang, Y., and Paxton, L. (2012). Daytime climatology of ionospheric nmf2 and hmf2 from cosmic data. *Journal of Geophysical Research: Space Physics*, 117(A09315).

[20] Calvert, W. and Schmid, C. W. (1964). Spread-F observations by the Alouette Topside Sounder Satellite. *Journal of Geophysical Research*, 69(9):1839–1852.

[21] Carter, B., Kellerman, A., Kane, T., Dyson, P., Norman, R., and Zhang, K. (2013). Ionospheric precursors to large earthquakes: A case study of the 2011 japanese tohoku earthquake. *Journal of Atmospheric and Solar-Terrestrial Physics*, 102:290–297.

[22] Carter, B., Yizengaw, E., Pradipta, R., Retterer, J., Groves, K., Valladares, C., Caton, R., Bridgwood, C., Norman, R., and Zhang, K. (2016a). Global equatorial plasma bubble occurrence during the 2015 st. patrick's day storm. *Journal of Geophysical Research: Space Physics*, 121(1):894–905.

[23] Carter, B., Yizengaw, E., Pradipta, R., Weygand, J., Piersanti, M., Pulkkinen, A., Moldwin, M., Norman, R., and Zhang, K. (2016b). Geomagnetically induced currents around the world during the 17 march 2015 storm. *Journal of Geophysical Research: Space Physics*, 121(10):10–496.

[24] Caruana, R., Lawrence, S., and Giles, C. L. (2001). Overfitting in neural nets: Backpropagation, conjugate gradient, and early stopping. In *Advances in Neural Information Processing Systems*, pages 402–408.

[25] Cesaroni, C., Spogli, L., Alfonsi, L., De Franceschi, G., Ciraolo, L., Monico, J. F. G., Scotto, C., Romano, V., Aquino, M., and Bougard, B. (2015). L-band scintillations and calibrated total electron content gradients over brazil during the last solar maximum. *Journal of Space Weather and Space Climate*, 5:A36.

[26] Chen, P. and Chen, J. (2014). The multi-source data fusion global ionospheric modeling software—ionogim. *Advances in Space Research*, 53(11):1610–1622.

[27] Chen, P., Yao, W., and Zhu, X. (2015). Combination of ground-and space-based data to establish a global ionospheric grid model. *IEEE Transactions on Geoscience and Remote Sensing*, 53(2):1073–1081.

[28] Chen, P., Yao, Y., and Yao, W. (2017). Global ionosphere maps based on gnss, satellite altimetry, radio occultation and doris. *GPS Solutions*, 21(2):639–650.

[29] Davies, K. (1990). *Ionospheric radio*. Number 31. IET.

[30] Depuev, V. and Pulinets, S. (2004). A global empirical model of the ionospheric topside electron density. *Advances in Space Research*, 34(9):2016–2020.

[31] Dyson, P. L. and Benson, R. F. (1978). Topside sounder observations of equatorial bubbles. *Geophysical Research Letters*, 5(9):795–798.

[32] Evans, J. (1969). Theory and practice of ionosphere study by Thomson scatter radar. *Proceedings of the IEEE*, 57(4):496–530.

[33] Fang, C., Chen, S., and Fuh, C. (2003). Automatic change detection of driving environments in a vision-based driver assistance system. *IEEE Transactions on Neural Networks*, 14(3):646–657.

[34] Farley Jr, D. (1963). A plasma instability resulting in field-aligned irregularities in the ionosphere. *Journal of Geophysical Research*, 68(22):6083–6097.

[35] Feltens, J. (2003). The international gps service (igs) ionosphere working group. *Advances in Space Research*, 31(3):635–644.

[36] Fu, E., Zhang, K., Wu, F., Xu, X., Marion, K., Rea, A., Kuleshov, Y., and Weymouth, G. (2007). An evaluation of gnss radio occultation technology for australian meteorology. *Positioning*, 1(11):0.

[37] Fu, E.-j., Zhang, K.-f., Marion, K.-y., Xu, X.-h., Marshall, J., Rea, A., Weymouth, G., and Kuleshov, Y. (2009). Assessing cosmic gps radio occultation derived atmospheric parameters using australian radiosonde network data. *Procedia Earth and Planetary Science*, 1(1):1054–1059.

[38] Glorot, X. and Bengio, Y. (2010). Understanding the difficulty of training deep feedforward neural networks. In *Proceedings of the Thirteenth International Conference on Artificial Intelligence and Statistics*, pages 249–256.

[39] Golub, G. H. and Van Loan, C. F. (1980). An analysis of the total least squares problem. *Journal on Numerical Analysis*, 17(6):883–893.

[40] Goncharenko, L., Salah, J., Van Eyken, A., Howells, V., Thayer, J., Taran, V., Shpynev, B., Zhou, Q., and Chau, J. (2005). Observations of the april 2002 geomagnetic storm by the global network of incoherent scatter radars. In *Annales Geophysicae*, volume 23, pages 163–181.

[41] Gordon, W. E. (1964). Arecibo ionospheric observatory. *Science*, 146:26–30.

[42] Gulyaeva, T. (2011). Storm time behavior of topside scale height inferred from the ionosphere–plasmasphere model driven by the F2 layer peak and GPS-TEC observations. *Advances in Space Research*, 47(6):913–920.

[43] Hagan, M. T., Demuth, H. B., Beale, M. H., et al. (1996). *Neural network design*, volume 20. Pws Pub. Boston.

[44] Hajj, G. A. and Romans, L. J. (1998). Ionospheric electron density profiles obtained with the Global Positioning System: Results from the GPS/MET experiment. *Radio Science*, 33(1):175–190.

[45] He, K., Zhang, X., Ren, S., and Sun, J. (2015). Delving deep into rectifiers: Surpassing human-level performance on imagenet classification. In *Proceedings of the IEEE International Conference on Computer Vision*, pages 1026–1034.

[46] Hernández-Pajares, M., Juan, J., and Sanz, J. (1999). New approaches in global ionospheric determination using ground gps data. *Journal of Atmospheric and Solar-Terrestrial Physics*, 61(16):1237–1247.

[47] Hernández-Pajares, M., Juan, J., Sanz, J., Orus, R., Garcia-Rigo, A., Feltens, J., Komjathy, A., Schaer, S., and Krankowski, A. (2009). The igs vtec maps: a reliable source of ionospheric information since 1998. *Journal of Geodesy*, 83(3-4):263–275.

[48] Hernández Pajares, M., Roma Dollase, D., Krankowski, A., García Rigo, A., and Orús Pérez, R. (2016). Comparing performances of seven different global vtec ionospheric models in the igs context. In *International GNSS Service Workshop (IGS 2016): Sydney, Australia: february 8-12, 2016*, pages 1–13. International GNSS Service (IGS).

[49] Hinton, G., Srivastava, N., and Swersky, K. (2012). Overview of mini-batch gradient descent. *Neural Networks for Machine Learning*.

[50] Hochegger, G., Nava, B., Radicella, S., and Leitinger, R. (2000). A family of ionospheric models for different uses. *Physics and Chemistry of the Earth, Part C: Solar, Terrestrial & Planetary Science*, 25(4):307–310.

[51] Hoque, M. and Jakowski, N. (2012). A new global model for the ionospheric f2 peak height for radio wave propagation. In *Annales Geophysicae*, volume 30, page 797. Copernicus GmbH.

[52] Hoque, M. M. and Jakowski, N. (2007). Higher order ionospheric effects in precise gnss positioning. *Journal of Geodesy*, 81(4):259–268.

[53] Hu, A., Carter, B., Julie, C., Norman, R., Wu, S., Wang, X., and Zhang, K. (2019a). Modeling of topside ionospheric vertical scale height based on ionospheric radio occultation measurements. *Journal of Geophysical Research: Space Physics*, 124(6):4926–4942.

[54] Hu, A., Li, Z., Carter, B., Wu, S., Wang, X., Norman, R., and Zhang, K. (2019b). Helmert-vce-aided fast-wtls approach for global ionospheric vtec modelling using data from gnss, satellite altimetry and radio occultation. *Journal of Geodesy*, 93(6):877–888.

[55] Hu, A., Wu, S., Wang, X., Wang, Y., Norman, R., He, C., Cai, H., and Zhang, K. (2018). Improvement of Reflection Detection Success Rate of GNSS RO Measurements Using Artificial Neural Network. *IEEE Transactions on Geoscience and Remote Sensing*, 56(2):760–769.

[56] Hu, A. and Zhang, K. (2018). Using bidirectional long short-term memory method for the height of f2 peak forecasting from ionosonde measurements in the australian region. *Remote Sensing*, 10(10):1658.

[57] Huo, X., Yuan, Y., Ou, J., Zhang, K., and Bailey, G. (2009). Monitoring the global-scale winter anomaly of total electron contents using gps data. *Earth, planets and space*, 61(8):1019–1024.

[58] Isham, B., Tepley, C., Sulzer, M., Zhou, Q., Kelley, M., Friedman, J., and González, S. (2000). Upper atmospheric observations at the arecibo observatory: Examples obtained using new capabilities. *Journal of Geophysical Research: Space Physics*, 105(A8):18609–18637.

[59] Krankowski, A., Zakharenkova, I., Krypiak-Gregorczyk, A., Shagimuratov, I. I., and Wielgosz, P. (2011). Ionospheric electron density observed by formosat-3/cosmic over the european region and validated by ionosonde data. *Journal of Geodesy*, 85(12):949–964.

[60] Kutiev, I. and Marinov, P. (2007). Topside sounder model of scale height and transition height characteristics of the ionosphere. *Advances in Space Research*, 39(5):759–766.

[61] Kutiev, I. S., Marinov, P. G., and Watanabe, S. (2006). Model of topside ionosphere scale height based on topside sounder data. *Advances in Space Research*, 37(5):943–950.

[62] Lei, J., Liu, L., Wan, W., and Zhang, S.-R. (2005). Variations of electron density based on long-term incoherent scatter radar and ionosonde measurements over Millstone Hill. *Radio Science*, 40(RS2008).

[63] Lei, J., Roble, R. G., Wang, W., Emery, B. A., and Zhang, S.-R. (2007a). Electron temperature climatology at Millstone Hill and Arecibo. *Journal of Geophysical Research: Space Physics*, 112(A02302).

[64] Lei, J., Syndergaard, S., Burns, A. G., Solomon, S. C., Wang, W., Zeng, Z., Roble, R. G., Wu, Q., Kuo, Y.-H., Holt, J. M., et al. (2007b). Comparison of cosmic ionospheric measurements with ground-based observations and model predictions: Preliminary results. *Journal of Geophysical Research: Space Physics*, 112(A07308).

[65] Li, L., Wu, S., Wang, X., Tian, Y., He, C., and Zhang, K. (2017). Seasonal multifactor modelling of weighted-mean temperature for ground-based gnss meteorology in hunan, china. *Advances in Meteorology*, 2017.

[66] Li, Z., Yuan, Y., Wang, N., Hernandez-Pajares, M., and Huo, X. (2015). Shpts: towards a new method for generating precise global ionospheric tec map based on spherical harmonic and generalized trigonometric series functions. *Journal of Geodesy*, 89(4):331–345.

[67] Lin, C., Richmond, A., Heelis, R., Bailey, G., Lu, G., Liu, J., Yeh, H., and Su, S.-Y. (2005). Theoretical study of the low-and midlatitude ionospheric electron density enhancement during the October 2003 superstorm: Relative importance of the neutral wind and the electric field. *Journal of Geophysical Research: Space Physics*, 110(A12312).

[68] Liu, C., Kirchengast, G., Zhang, K., Norman, R., Li, Y., Zhang, S., Fritzer, J., Schwaerz, M., Wu, S., and Tan, Z. (2015). Quantifying residual ionospheric errors in gnss radio occultation bending angles based on ensembles of profiles from end-to-end simulations. *Atmospheric Measurement Techniques*, 8(7):2999–3019.

[69] Liu, L., He, M., Wan, W., and Zhang, M.-L. (2008). Topside ionospheric scale heights retrieved from Constellation Observing System for Meteorology, Ionosphere, and Climate radio occultation measurements. *Journal of Geophysical Research: Space Physics*, 113(A10304).

[70] Liu, L., Le, H., Wan, W., Sulzer, M. P., Lei, J., and Zhang, M.-L. (2007). An analysis of the scale heights in the lower topside ionosphere based on the arecibo incoherent scatter radar measurements. *Journal of Geophysical Research: Space Physics*, 112(A06307).

[71] Magdaleno, S., Altadill, D., Herraiz, M., Blanch, E., and de La Morena, B. (2011). Ionospheric peak height behavior for low, middle and high latitudes: A potential empirical model for quiet conditions—comparison with the iri-2007 model. *Journal of Atmospheric and Solar-Terrestrial Physics*, 73(13):1810–1817.

[72] Mahajan, K. and Pandey, V. (1979). Solar activity changes in the electron temperature at 1000-km altitude from the Langmuir probe measurements on Isis 1 and Explorer 22 satellites. *Journal of Geophysical Research: Space Physics*, 84(A10):5885–5889.

[73] Mannucci, A., Wilson, B., Yuan, D., Ho, C., Lindqwister, U., and Runge, T. (1998). A global mapping technique for gps-derived ionospheric total electron content measurements. *Radio Science*, 33(3):565–582.

[74] Marquardt, D. W. (1963). An algorithm for least-squares estimation of nonlinear parameters. *Journal of the Society for Industrial and Applied Mathematics*, 11(2):431–441.

[75] Ng, A. Y. (2004). Feature selection, l 1 vs. l 2 regularization, and rotational invariance. In *Proceedings of the Twenty-first International Conference on Machine Learning*, page 78. ACM.

[76] Ngwira, C. M., McKinnell, L.-A., Cilliers, P. J., and Coster, A. J. (2012). Ionospheric observations during the geomagnetic storm events on 24–27 july 2004: Long-duration positive storm effects. *Journal of Geophysical Research: Space Physics*, 117(A9).

[77] Pavelyev, A., Liou, Y., Zhang, K., Wang, C., Wickert, J., Schmidt, T., Gubenko, V., Pavelyev, A., and Kuleshov, Y. (2012). Identification and localization of layers in the ionosphere using the eikonal and amplitude of radio occultation signals. *Atmospheric Measurement Techniques*, 5(1):1–16.

[78] Plan, S. (1995). National space weather program strategic plan. *FCM˜P30-1995, Office of the Federal Coordinator for Meteorological Services and Supporting Research, Silver Springs, MD*.

[79] Prolss, G. W. and Bird, M. K. (2004). *Physics of the Earth's space environment: an introduction*. Springer.

[80] Pullen, S., Park, Y. S., and Enge, P. (2009). Impact and mitigation of ionospheric anomalies on ground-based augmentation of gnss. *Radio Science*, 44(1).

[81] Reinisch, B., Nsumei, P., Huang, X., and Bilitza, D. (2007). Modeling the F2 topside and plasmasphere for IRI using IMAGE/RPI and ISIS data. *Advances in Space Research*, 39(5):731–738.

[82] Richards, P. (2001). Seasonal and solar cycle variations of the ionospheric peak electron density: Comparison of measurement and models. *Journal of Geophysical Research: Space Physics*, 106(A7):12803–12819.

[83] Richards, P., Meier, R., and Wilkinson, P. (2010). On the consistency of satellite measurements of thermospheric composition and solar EUV irradiance with Australian ionosonde electron density data. *Journal of Geophysical Research: Space Physics*, 115(A10309).

[84] Roberts, C., Zhang, K., Rizos, C., Kealy, A., Ge, L., Ramm, P., Hale, M., Kinlyside, D., and Harcombe, P. (2004). Improved atmospheric modelling for large scale high-precision positioning based on gnss cors networks in australia. *Positioning*, 1(08):0.

[85] Rocken, C., Anthes, R., Exner, M., Hunt, D., Sokolovskiy, S., Ware, R., Gorbunov, M., Schreiner, W., Feng, D., Herman, B., et al. (1997). Analysis and validation of GPS/MET data in the neutral atmosphere. *Journal of Geophysical Research: Atmospheres*, 102(D25):29849–29866.

[86] Rohm, W., Yuan, Y., Biadeglgne, B., Zhang, K., and Le Marshall, J. (2014). Ground-based gnss ztd/iwv estimation system for numerical weather prediction in challenging weather conditions. *Atmospheric Research*, 138:414–426.

[87] Ruder, S. (2016). An overview of gradient descent optimization algorithms. *arXiv preprint arXiv:1609.04747*.

[88] Sai Gowtam, V. and Tulasi Ram, S. (2017). An artificial neural network-based ionospheric model to predict nmf2 and hmf2 using long-term data set of formosat-3/cosmic radio occultation observations: Preliminary results. *Journal of Geophysical Research: Space Physics*, 122(11):743–755.

[89] Schaffrin, B. and Wieser, A. (2008). On weighted total least-squares adjustment for linear regression. *Journal of Geodesy*, 82(7):415–421.

[90] Schalkoff, R. J. (1997). *Artificial neural networks*, volume 1. McGraw-Hill New York.

[91] Schreiner, W., Rocken, C., Sokolovskiy, S., Syndergaard, S., and Hunt, D. (2007). Estimates of the precision of GPS radio occultations from the COSMIC/FORMOSAT-3 mission. *Geophysical Research Letters*, 34(L04808).

[92] Schreiner, W. S., Sokolovskiy, S. V., Rocken, C., and Hunt, D. C. (1999). Analysis and validation of GPS/MET radio occultation data in the ionosphere. *Radio Science*, 34(4):949–966.

[93] Schuster, M. and Paliwal, K. K. (1997). Bidirectional recurrent neural networks. *IEEE Transactions on Signal Processing*, 45(11):2673–2681.

[94] Shen, Y., Li, B., and Chen, Y. (2011). An iterative solution of weighted total least-squares adjustment. *Journal of Geodesy*, 85(4):229–238.

[95] Shim, J., Kuznetsova, M., Rastätter, L., Hesse, M., Bilitza, D., Butala, M., Codrescu, M., Emery, B., Foster, B., Fuller-Rowell, T., et al. (2011). CEDAR electrodynamics thermosphere ionosphere (ETI) challenge for systematic assessment of ionosphere/thermosphere models: NmF2, hmF2, and vertical drift using ground-based observations. *Space Weather*, 9(S12003).

[96] Shubin, V., Karpachev, A., and Tsybulya, K. (2013). Global model of the f2 layer peak height for low solar activity based on gps radio-occultation data. *Journal of Atmospheric and Solar-Terrestrial Physics*, 104:106–115.

[97] Sokolovskiy, S. and Rocken, C. (2006). Algorithms for inverting radio occultation signals in the neutral atmosphere. *University Corporation for Atmospheric Research*.

[98] Srivastava, N., Hinton, G., Krizhevsky, A., Sutskever, I., and Salakhutdinov, R. (2014). Dropout: a simple way to prevent neural networks from overfitting. *The Journal of Machine Learning Research*, 15(1):1929–1958.

[99] Stankov, S. M., Jakowski, N., Heise, S., Muhtarov, P., Kutiev, I., and Warnant, R. (2003). A new method for reconstruction of the vertical electron density distribution in the upper ionosphere and plasmasphere. *Journal of Geophysical Research: Space Physics*, 108(A5).

[100] Stolle, C., Jakowski, N., Schlegel, K., and Rietveld, M. (2004). Comparison of high latitude electron density profiles obtained with the gps radio occultation technique and eiscat measurements. In *Annales Geophysicae*, volume 22, pages 2015–2022.

[101] Taylor, J. W. and Buizza, R. (2002). Neural network load forecasting with weather ensemble predictions. *IEEE Transactions on Power Systems*, 17(3):626–632.

[102] Thome, G. D. (1964). Incoherent scatter observations of traveling ionospheric disturbances. *Journal of Geophysical Research*, 69(19):4047–4049.

[103] Titheridge, J. (1998). Temperatures in the upper ionosphere and plasmasphere. *Journal of Geophysical Research: Space Physics*, 103(A2):2261–2277.

[104] Todorova, S., Hobiger, T., and Schuh, H. (2008). Using the global navigation satellite system and satellite altimetry for combined global ionosphere maps. *Advances in Space Research*, 42(4):727–736.

[105] Truhlik, V., Bilitza, D., and Triskova, L. (2009). Latitudinal variation of the topside electron temperature at different levels of solar activity. *Advances in Space Research*, 44(6):693–700.

[106] Truhlik, V., Bilitza, D., and Triskova, L. (2012). A new global empirical model of the electron temperature with the inclusion of the solar activity variations for IRI. *Earth, Planets and Space*, 64(6):531–543.

[107] Truhlík, V., Třísková, L., and Šmilauer, J. (2001). Improved electron temperature model and comparison with satellite data. *Advances in Space Research*, 27(1):101–109.

[108] Truhlik, V., Třísková, L., Šmilauer, J., and Afonin, V. (2000). Global empirical model of electron temperature in the outer ionosphere for period of high solar activity based on data of three intercosmos satellites. *Advances in Space Research*, 25(1):163–169.

[109] Tulasi Ram, S., Sai Gowtam, V., Mitra, A., and Reinisch, B. (2018). The improved two-dimensional artificial neural network-based ionospheric model (annim). *Journal of Geophysical Research: Space Physics*, 123(7):5807–5820.

[110] Webb, P. and Essex, E. (2003). Modifications to the titheridge upper ionosphere and plasmasphere temperature model. *Journal of Geophysical Research: Space Physics*, 108(A10).

[111] Wen, D., Yuan, Y., Ou, J., Zhang, K., and Liu, K. (2008). A hybrid reconstruction algorithm for 3-d ionospheric tomography. *IEEE Transactions on Geoscience and Remote Sensing*, 46(6):1733–1739.

[112] Wu, S., Zhang, K., Yuan, Y., and Wu, F. (2006). Spatio-temporal characteristics of the ionospheric tec variation for gpsnet-based real-time positioning in victoria. *Positioning*, 1(10):0.

[113] Yan, S., Li, Z., Yu, K., and Zhang, K. (2014). GPS-R L1 interference signal processing for soil moisture estimation: an experimental study. *EURASIP Journal on Advances in Signal Processing*, 2014(1):107.

[114] Yuan, Y., Li, Z., Wang, N., Zhang, B., Li, H., Li, M., Huo, X., and Ou, J. (2015). Monitoring the ionosphere based on the crustal movement observation network of china. *Geodesy and Geodynamics*, 6(2):73–80.

[115] Yuan, Y., Zhang, K., Rohm, W., Choy, S., Norman, R., and Wang, C.-S. (2014). Real-time retrieval of precipitable water vapor from gps precise point positioning. *Journal of geophysical research: atmospheres*, 119(16):10044–10057.

[116] Yue, X., Schreiner, W. S., Lin, Y.-C., Rocken, C., Kuo, Y.-H., and Zhao, B. (2011). Data assimilation retrieval of electron density profiles from radio occultation measurements. *Journal of Geophysical Research: Space Physics*, 116(A03317).

[117] Zhang, K., Fu, E., Xu, H., Liou, Y., Le Marshall, J., and Kuleshov, Y. (2009). A study of collocation criteria of gnss cosmic radio occultation and radiosonde comparisons. In *IGNSS Symposium 2009*, pages 1–9. International Global Navigation Satellite Systems Society.

[118] Zhang, K., Manning, T., Wu, S., Rohm, W., Silcock, D., and Choy, S. (2015). Capturing the signature of severe weather events in australia using gps measurements. *IEEE Journal of Selected Topics in Applied Earth Observations and Remote Sensing*, 8(4):1839–1847.

[119] Zhang, S., Holt, J. M., Zalucha, A. M., and AmoryMazaudier, C. (2004). Midlatitude ionospheric plasma temperature climatology and empirical model based on Saint Santin incoherent scatter radar data from 1966 to 1987. *Journal of Geophysical Research: Space Physics*, 109(A11311).

[120] Zhang, S., Oliver, W. L., Holt, J. M., and Fukao, S. (2003). Ionospheric data assimilation: Comparison of extracted parameters using full density profiles and key parameters. *Journal of Geophysical Research: Space Physics*, 108(A3,1131).

[121] Zhao, H., Yao, M., Deng, X., Yuan, K., Ding, F., Zeng, L., and Li, C. (2018). Antenna array simulation and detection performance analysis of sanya prototype incoherent scatter radar. *Radio Science*, 53(6):820–829.

[122] Zhou, Q. H. and Sulzer, M. P. (1997). Incoherent scatter radar observations of the f-region ionosphere at arecibo during january 1993. *Journal of Atmospheric and Solar-Terrestrial Physics*, 59(17):2213–2229.